LOCATING A MOVING TARGET IN A HIGH CLUTTER ENVIRONMENT

By

ERNEST DAVID GENTRY

Bachelor of Science in Electrical Engineering

Oklahoma State University

Stillwater, OK

2007

Submitted to the Faculty of the
Graduate College of the
Oklahoma State University
in partial fulfillment of
the requirements for
the Degree of
MASTER OF SCIENCE
May, 2010

LOCATING A MOVING TARGET IN A HIGH

CLUTTER ENVIRONMENT

Thesis Approved:

Dr. James West

Thesis Adviser

Dr. Charles Bunting

Dr. George Scheets

Dr. Damon Chandler

Dr. Mark E. Payton

Dean of the Graduate College

ACKNOWLEDGMENTS

I would like to thank my graduate thesis advisor, Dr. West. He provided useful insight and knowledge throughout my academic career. He helped steer me back on course whenever my research would go off on a tangent. He gave me just enough information at times to make me think about the problem and apply my own solutions. He kept the standard high in all of the classes I took with him, expanding my knowledge and understanding of topics related to electricity and magnetism. If I had to repeat my graduate career again, I would still pick Dr. West as my thesis advisor.

I would also like to thank my family and friends who provided support while I was in school. I, especially, would like to thank my wife. She had to endure several late nights of me staying up late working on homework, collecting data for my thesis, or writing on my thesis. I am also thankful for her patience. She had to listen and endure many talks ranging from math and science to my current work on my thesis. I would like to thank my dad for always instilling in me the importance of getting a higher education degree. He was always telling me to get a higher education degree and to not just stop at a bachelor's degree, but pursue a master's degree as well. And I would like to thank all my other family member's, my mom, my sister, Charla, my grandparents, my aunt Debbie and uncle Robert, my cousin, Danny, my in-laws, Bill and Pat, Chris and Maddie, and Tim and Kari, my nieces and nephews, MichaelRyan and Alyssa, Robert, MytheAnn, Morgan and Evan, Buddy, Katie, and Iysis, who were very understanding, for not getting upset at me if I ignored them unintentionally. There would be times when they would come and visit and I would have a project or homework assignment would be due the next day preventing me from spending any time with them.

I would like to thank Vignesh Rajamani, who now has a doctorate degree in electrical engineering. He provided me with useful information about how to use the equipment and how to take reverb chamber measurements. He also provided an ear and feedback when I was needing someone to listen to me when coming up with different thesis ideas.

I would like to thank Dr. Bunting for providing me an opportunity to increase my knowledge of microwave networks by helping create a revised Microwave Engineering course that had projects related to the theory. I would also like to thank him for stressing the importance of learning MATLAB in my undergraduate academic career. The difficulty of several of my graduate courses would have increased had I not learned MATLAB during my undergraduate studies. I also owe him a debt of gratitude for helping fund my graduate studies.

I would like to thank Nick Oswald, David Green, and Robert Diehl for helping me with taking measurements for my thesis. I really appreciated the time they volunteered to help me. Had they not helped me out several of the measurements would have taken several hours longer to complete.

I would like to thank everyone else who helped me out with my academic career whether it was a professor or a staff member. I would like to personally thank all of these people whose names appear in random order according to who pops into my head first. I thank Dr. Bell, Dr. Scheets, Dr. Chandler, Ron Knight, Helen Daggs, Lory Ferguson, Dr. Hagan, Mr. Griffin, Dr. Young, Dr. Miller, and Dr. Latino.

TABLE OF CONTENTS

LIST OF FIGURES

ACRONYM LIST

BW	Bandwidth
DAQ	Data Acquisition Device
EM	Electromagnetic
FT	Fourier Transform
FFT	Fast-Fourier Transform
FMCW	Frequency-Modulated Continuous Wave
FSCW	Frequency-Stepped Continuous Wave
GUI	Graphical User Interface
I Channel	In-Phase Channel
IFT	Inverse-Fourier Transform
IFFT	Inverse Fast-Fourier Transform
MTI	Moving Target Indicator
OSU-UML	Oklahoma State University – University Multispectral Laboratories
PBR	Passive Bistatic Radar
PRF	Pulse Repetition Frequency
Q Channel	Quadrature Channel
RCS	Radar Cross Section
RF	Radio Frequency
SAR	Synthetic Aperture Radar
SNR	Signal-to-Noise Ratio
VNA	Vector Network Analyzer

ABSTRACT

This paper addresses the problem of locating a slowly moving target, such as a human being, in a high clutter environment. The test uses a vector network analyzer (VNA) as a radar system. The radar system is operated as a frequency-stepped continuous wave (FSCW) radar. The real and imaginary amplitude values of the S21 parameter are recorded for each frequency step. The inverse fast-Fourier transform (IFFT) is then applied to the complex S21 data to recover the time domain returns from a room or hallway. The target is located using a variable pulse repetition frequency (PRF) moving target indicator (MTI) filter. A reference pulse of the room or hallway was acquired, initially, with no target present. Consecutive pulses were then measured with the target present in the room or hallway. After each pulse, the target was moved 3 ft and a new measurement was saved. This process was repeated for each target. Targets included a corner reflector, a sphere, and a human subject.

The results showed that the variable PRF, single-stage, MTI filter effectively identified the presence of a target in a high clutter environment for all three target cases. Subtracting a reference pulse from the pulses when a target was present in the room or hallway suppressed most of the background clutter. There were some returns from strong reflection points in the room or hallway that still appeared in the filter returns, however. This was due to either the target intercepting and scattering the energy that would otherwise reflect from the background or the range cells of the background return signals being moved due to multipath.

This test demonstrated that use of a reference pulse in a variable PRF MTI filter allowed the detection of a slowly moving target. Future work will be needed to address the issue of strong reflection points appearing after filtering. Possible solutions include addition of a second MTI stage to the processing.

CHAPTER 1

INTRODUCTION

There have been several techniques developed that track the movement of slowly moving targets in a high clutter environment. For example, in Zhou et al [3], Okada et [4], and Boult et al [5] a camera system was employed to detect the movement of objects. Chetty et al [1] used a passive bistatic radar system where the radar signal used was the WiFi network setup in the building. Ahmad [2], also, used a radar system except that it tried forming three dimensional synthetic aperture radar (SAR) images. Richards [6] and Levanon [7] discussed different Doppler processing techniques used to locate a moving target. All of these techniques did provide useful information about detecting a moving target. More importantly, they offered different ways to detect a human being walking in a high clutter environment.

Camera systems do offer a nice visual reference for locating a moving target. Zhou et al [3], for instance, used human gait to detect movement by using a Bayesian and neural network model. Using the strong prior information from a video database, Zhou et al [3] created a two dimensional walker model that took into account the types of clothing a walker might be wearing such as a trench coat or skirt. Zhou et al [3], also, took all video images of the fronto-parallel (side-view) side of the walker. There were several downsides to this approach. Firstly, none of the results were processed in real-time because of the computational complexity. Secondly, prior information was required for this model to work so the neural network could learn and have a comparative base. Lastly, the model started breaking down when the walker was partially obstructed by an object such as a bush or tree.

Okada's [4] approach also used a camera system, but it used a different approach compared to Zhou's [3]. Okada et al [4] actually had a camera mounted on top of a servo motor that would move to track the movement of the human target. First, Okada [4] located a moving object by performing a simple background subtraction on each image frame from a reference image. Whenever a certain number of pixels were above a defined threshold, the rest of the camera system activated. Once activated, the camera would always keep the object at the center of the field of view for the camera. Okada's [4] technique would determine which direction the target was going with respect to the camera. Then, a command would be sent to the servo to update its position thus effectively tracking the target. The drawback with this method was the amount of computational power required to make this a real-time system. Two computers were required. One computer was solely dedicated to image processing while the other computer controlled the servo motor. Another drawback was the flicker of the lights in the hallway. This

would change the intensity values of the images affecting the pixel values of the target. This could result in a missed target because several of the pixel values were below the threshold.

Boult's [5] approach for detecting a target was similar to Okada et al [4], but more effort was devoted to keeping a constant false alarm rate. Like Okada et al [4], Boult et al [5] detected the presence of a target by first subtracting the current image from the reference image. Then, thresholding was performed to determine what pixels included the target. What was different was Boult et al [5] always updated the reference image by performing an *up*-down model, a conditional increment model. The purpose of the up-down model was to take into consideration the changes in the background scenery that would occur throughout the day. If the background images pixels were greater than the current images pixels an update parameter was subtracted from the background image pixel. If the background image pixel was smaller, the update parameter was added to the background image pixel. If neither condition was satisfied the background image pixel was not updated. Since the reference image was continually updated, an algorithm was developed that set the pixel threshold value to be dynamic. The main drawback to this method was when looking for a low contrast camouflaged target it could not detect the target until it was 20-25 meters away from the camera. At that distance the target, for example, a sniper, could find a way to disrupt surveillance.

When using radar systems to detect a moving target there are several different detection schemes that could be employed. Chetty et al [1] decided to use a passive bistatic radar (PBR) setup inside a building to look for movement. This system worked by pointing one antenna directly at the WiFi beacon to provide a reference and correlation signal, with the other scattered signals picked up from the other antennas placed in the building [1]. Once enough coherent phase data was collected from the antennas, an ambiguity function was applied to reveal the range and velocity of the moving target. Even though the approach was interesting, there were problems. If any of the passive antennas in the PBR system picked up any direct signal interference from the WiFi beacon, it would provide strong correlation with the reference signal creating large sidelobes in the range and Doppler axes which would drown out any weak signal returns due to an actual target [1]. Another disadvantage to PBR was poor range resolution. Since the data bit stream from the WiFi signal only has 16 MHz that gives a range resolution of approximately 30 ft which makes it hard for the PBR system to detect multiple targets in a room [1]. Another issue with using a PBR setup was the amount of cabling and antennas needed to make an effective surveillance system in a building which could easily make the cost of the system sky-rocket.

Another radar system that could be used as a surveillance system inside a building was the system discussed in [2]. In [2], it was proposed that a SAR image could be made of the room of interest. The radar system could be placed next to an exterior wall in another room and moved left, right, up, or down to create an image. The signal would be stepped through several frequencies to perform range compression in the z axis. Then the radar would either be moved up or down and left or right to create the y and x dimensions of the image of the room. Once all of the data was collected, the three-dimensional volume image would be reconstructed from

the phase data. Then a thresholding was performed on each voxel (a three-dimensional pixel) to determine if a target was present in the room. There were several shortcomings with this approach. The most noticeable one was the fact that the radar system actually had to be moved to create the image. If the operator was not precise with his or her movements it would degrade the system performance of the radar. Other factors that would degrade system performance were the uncertainties of the wall parameters, multiple walls, and non-uniform walls. Another difficult shortcoming to overcome was target interactions with the room and multipath issues. Both of these problems would create false targets in the imagery data.

It was originally proposed for this work that Doppler processing would be used to detect the presence of a moving target in a high clutter environment. Since the radar system would be used inside a building where it was assumed that all clutter would be stationary, the Doppler spectrum for the clutter would all be at zero Hertz. It was thought that all that would be required is a radar system that would pulse several times, recording the phase information for the range bins. Then the fast-Fourier Transform (FFT) would be applied across all pulses for each range bin [6], [7]. Any range bin values that showed a Doppler shift in the Doppler spectrum plot would indicate the presence of a moving target. Since it was understood that any target moving inside a building would be a slowly moving target, the associated Doppler shift of the moving target would be near zero Hertz. The problem with this approach was, according to [6] and [7], a finer Doppler frequency resolution require more pulses to be taken. Otherwise, having a coarser Doppler resolution could result in the target's Doppler shift being grouped together with the zero Hertz clutter Doppler spectrum, preventing any detection of a very slowly moving target. Also, [6] and [7] stated that increasing the Doppler resolution increases the dwell time to take into account the extra pulses taken. If the target is able to exit the hallway within one dwell time of the radar system, then the radar operator would think that the blip on the screen was a false alarm. Thus, allowing detection of slowly moving targets allows quickly moving targets to evade detection, and vice versa.

The new proposal that would replace the pulse Doppler processing problem was a variable pulse repetition frequency (PRF) using a single-stage canceller moving target indicator (MTI) filter. The radar would continuously send out pulses subtracting the previous pulse from a reference pulse until a target was detected. Any range bins that were above a specific threshold would be detected as a target and their range value would be recorded and plotted on a graph indicating the location of the target in the hallway. Every 15 minutes or more, the reference pulse would be updated depending on the coherency of the entire system.

Chapter 2 discusses the theory and operation of the radar system. Chapter 3 goes through the system setup and verification of the radar system operation. Chapter 4 gives the results of the radar system while chapter 5 concludes the project and discusses successes and future work that would enhance the performance of the radar system.

REFERENCES

[1] Kevin Chetty, Graeme Smith, Hui Guo, and Karl Woodbridge, “Target Detection in High Clutter using Passive Bistatic Wifi Radar,” Radar Conference, IEEE 2009, pp. 1-5.

[2] Fauzia Ahmad, “Multi-Location Wideband Through the Wall Beamforming,” ICASSP, IEEE 2008, pp 5193-5196.

[3] Ziheng Zhou, Adam Prügel-Bennet, Robert I. Damper, “A Bayesian for Extracting Human Gait Framework Using Strong Prior Knowledge,’ IEEE Transactions on PAMI, IEEE 2006, pp.1738-1752.

[4] Ryuzo Okada, Junji Oaki, Daisuke Yamamoto, Nobuhiro Kondoh, Hiroshi Miyazaki, Koki Uesugi, Jiro Amemiya, Kenji Shirakawa, and Atsushi Kunimatsu, “High-speed Object Tracking in Ordinary Surroundings Based on Temporally Evaluated Optical Flow,” Intl. Conference on Intelligent Robots and Systems (ICIRS 2003), IEEE Proceedings, 2003, pp. 242-247.

[5] Terrance E. Boult, Ross J. Michaels, Xiang Gao, and Michael Eckmann, “Into the Woods: Visual Surveillance of Noncooperative and Camouflaged Targets in Complex Outdoor Settings,” Proceedings of IEEE, IEEE 2001, pp.1382-1402.

[6] Mark A. Richards, *Fundamentals of Radar Signal Processing,* McGraw-Hill, 2005.

[7] Nadav Levanon, *Radar Principles*, John Wiley and Sons, 1988.

CHAPTER 2

RADAR SYSTEM THEORY AND OPERATION

The radar system will be operated as a frequency-stepped continuous wave (FSCW) radar. The radar will measure the range of the objects by sampling the phase in the frequency domain and transform the phase data back to the time domain to recover the target delay of the signal by taking the inverse Fourier transform (IFT) [1], [2], [3]. The presence of a target is determined by comparing an earlier recovered pulse with the current pulse. This is known as single stage moving target indicator (MTI) processing [1], [2], [3], implemented here with a variable delay between the current and reference pulse. If there is a change in the range-resolved information between the two pulses, then the radar system would notify the radar operator that there is movement in the hallway. The vector network analyzer (VNA) will be used as the signal source and receiver for the test radar system used here.

Taking the IFT of the phase data is equivalent to pulse compression and matched filtering. Therefore, the sections in this chapter will review matched filtering and pulse compression. The sections will also discuss how these techniques are implemented in the radar system.

MATCHED FILTER

The term matched filter is a communication term used for describing the filter network of the receiver [4]. Ideally, the filter network's frequency response would be the complex conjugate of the received signals spectrum. The benefit of only allowing the received signals frequency components through the receiver is that all of other frequencies that enter the receiver, such as noise, are suppressed if they do not share the same frequency spectrum. The effect of suppressing the other frequencies is it optimizes the signal to noise ratio (SNR). So, for a radar system this could possibly mean an increase in the maximum range for detection, a higher probability of detection, or both.

One example of an analog radar system that operates as a matched filter detector is a frequency modulation continuous wave (FMCW) radar. FSCW operation is similar to FMCW with the

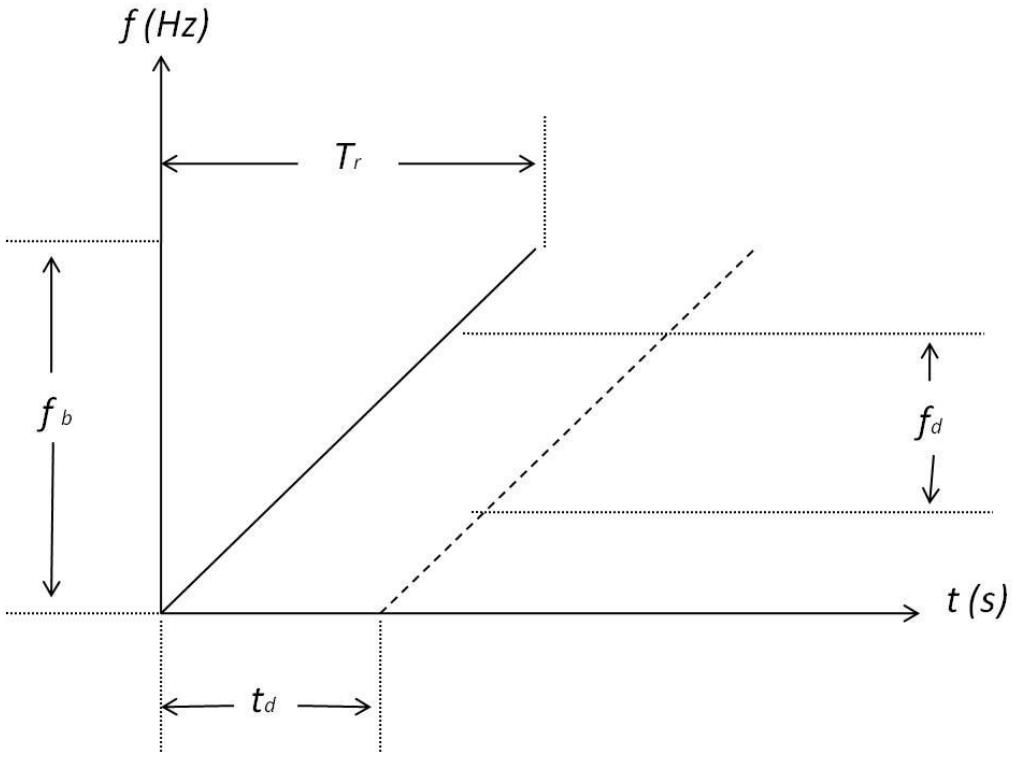

Figure 2–1: Frequency versus time plot of both the transmitted and received signal for an FMCW radar.

exception that the frequency is being stepped discretely. Both techniques take advantage of matched filtering. However, the matched filtering technique for FSCW does not happen until the IFT of the frequency domain is taken. Since both FMCW and FSCW are similar, a review will be given of FMCW as an example to reinforce matched filtering concepts.

An FMCW radar operates by continuously sweeping from a start frequency to a stop frequency. Figure 2–1 shows the frequency versus time plot for the FMCW radar. As can be seen from the figure, the first ramp (on the left) is the transmitted signal coming from the signal generator while the second ramp (on the right) is the received reflected signal from the target. It is this plot that helps in visualizing how the radar measures the range of the target. The difference frequency variable, f_d, is the output frequency from the mixer and is used to calculate the range. So, the larger the time delay, t_d, of the reflected signal the larger the difference frequency resulting in a larger target range. Equation (1) shows the relationship between all the variables and how the range of the target is determined [1]:

$$f_d = {(2 * R * f_b)}\Big/{(T_r * c)} \tag{1}$$

The variables f_b, T_r , R, and c are the frequency sweep bandwidth, the sweep time, the target range, and the speed of light in a vacuum.

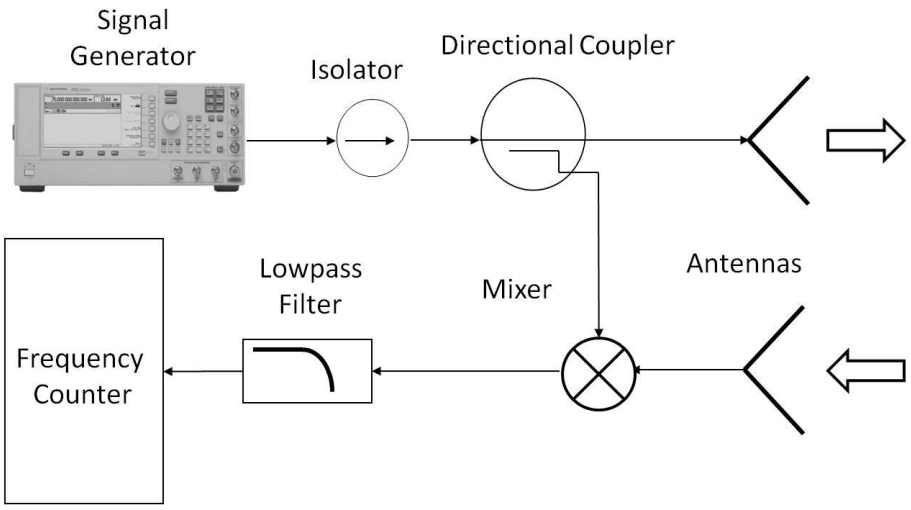

Figure 2–2: Matched filter detector circuit.

Figure 2–3 and Figure 2–4 show the time domain plot of an FMCW sweep and its matched filter output. MATLAB code for generating these plots is found in Appendix A. Figure 2–5 and Figure 2–6 represent the time domain amplitude plots of the transmitted and received signals for a standard FMCW sweep. It is assumed that as the signal generator is sweeping in frequency the amplitude of the transmitted signal remains constant, making the amplitude plot resemble a frequency modulated pulse waveform as shown in Figure 2–5. If there is no distortion in the received signal, it is assumed that the reflected signal's shape is identical to the transmitted signals shape, but with a different amplitude value.

Figure 2–2 shows the microwave circuit that would be used to implement an analog matched filter. The only microwave components that would be needed to build the analog matched filter would be two antennas, an isolator, a directional coupler, a frequency mixer, and a lowpass filter. The only other items needed to run the circuit would be an RF signal generator and a frequency counter. To explain how this circuit represents a matched filter, a brief discussion about how the signal propagates through the circuit is first given. The signal starts from the signal generator, passes through the isolator, and then goes through the directional coupler with part of the signal sampled and directed towards the mixer. It then exits out the antenna looking for a target. The reflected signal enters the system through the bottom antenna and arrives at the mixer where it is then multiplied by the original transmitted signal. The output of the mixer then is passed through a lowpass filter to filter out the harmonic frequencies generated by the mixer. From there the signal is sampled by the frequency counter. It is the multiplication of these two waveforms at the input to the mixer that performs the matched filtering. In the time domain the system response for the matched filter detector of an impulse waveform is a mirrored time-delayed version of the waveform itself as seen in Figure 2–6 [3]. The mixer, however, only mathematically represents the equivalent of a matched filter. The mirrored response is never explicitly used.

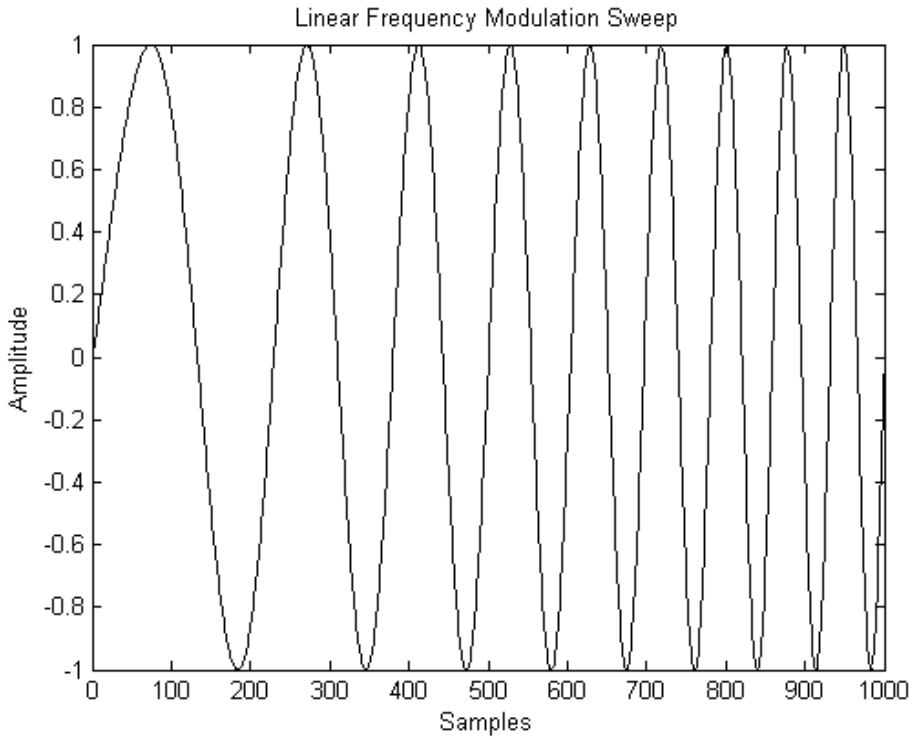

Figure 2–3: Plot of a linear frequency modulation sweep function.

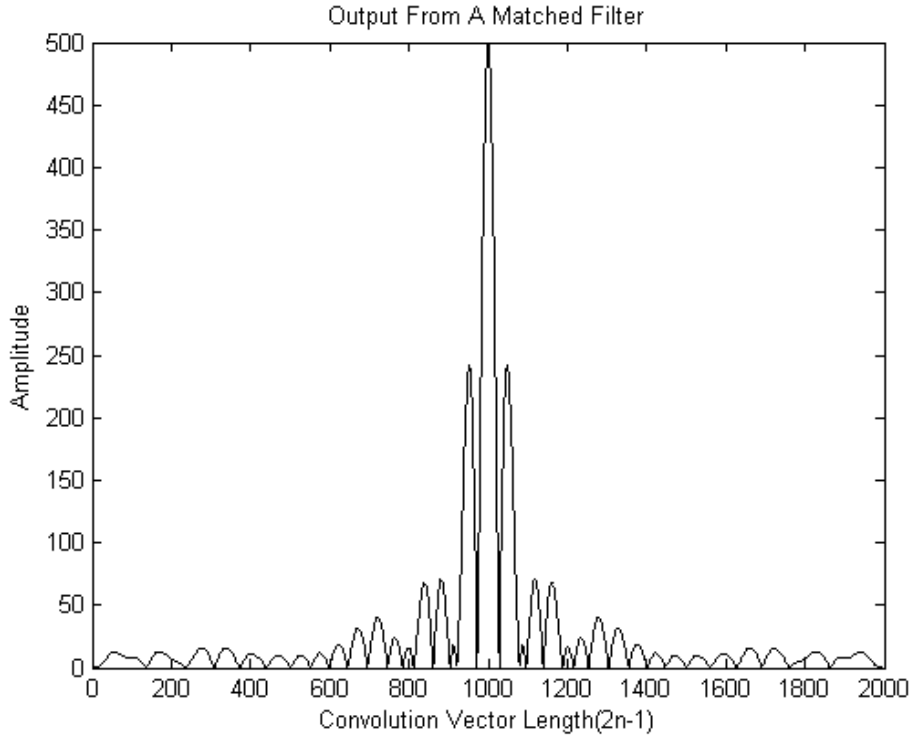

Figure 2–4: Plot of the output of a matched filter for an FMCW sweep.

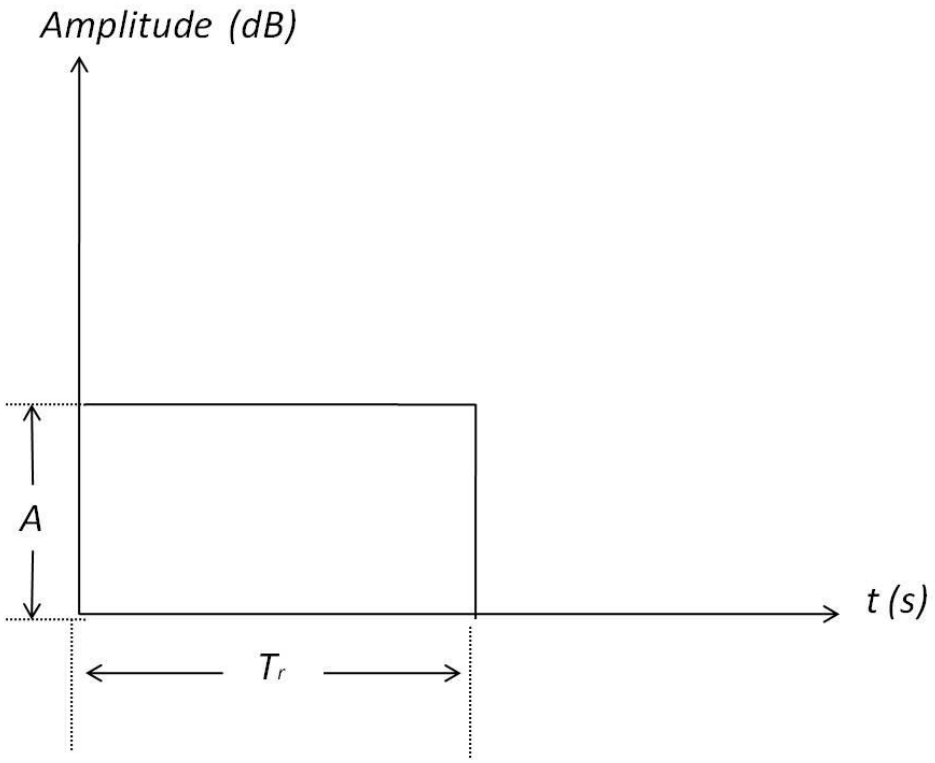

Figure 2–5: Time domain amplitude plot of the transmitted signal during a FMCW sweep.

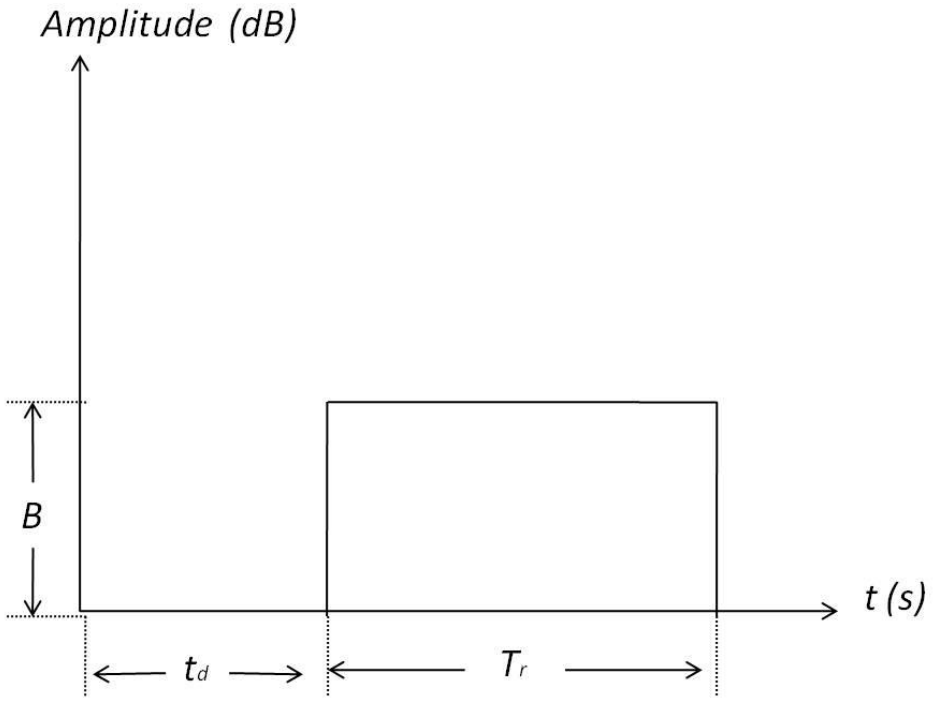

Figure 2–6: Time domain amplitude plot of the received signal during an FMCW sweep.

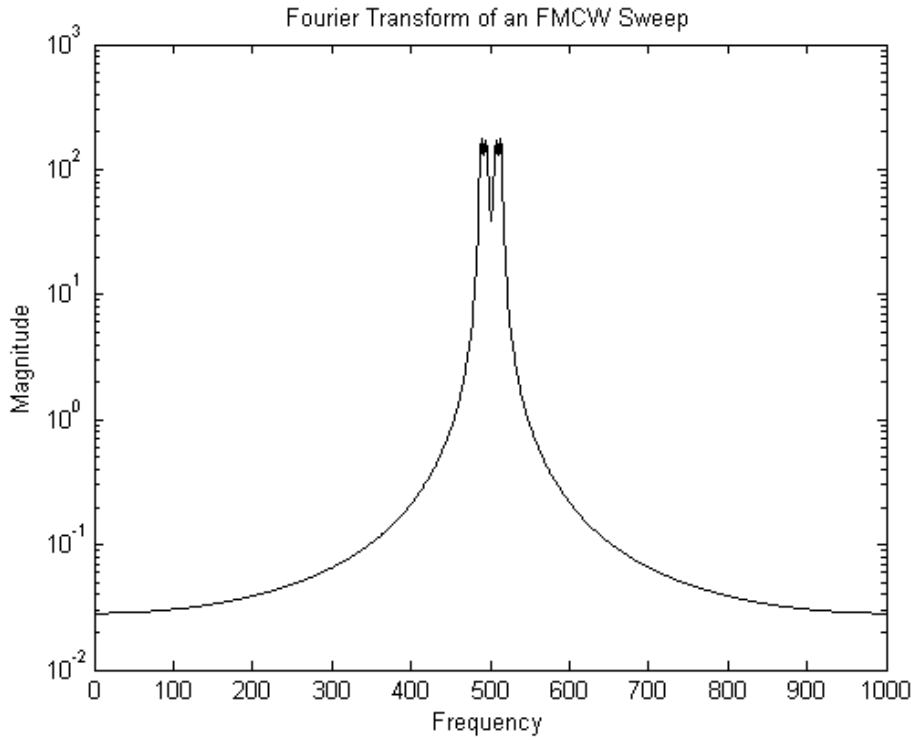

Figure 2–7: Semilog plot of the fast-Fourier Transform of an FMCW sweep using MATLAB.

PULSE COMPRESSION

Figure 2–7 shows the fast-Fourier transform (FFT) of the FMCW sweep shown in Figure 2–3. Code for generating this plot can be found in Appendix A. As mentioned in the previous section, taking the complex conjugate of Figure 2–7 creates the matched filter transfer function of the FMCW sweep. To perform the matched filtering, the received signals transfer function would be multiplied by the matched filter. At the output of the matched filter, the inverse fast-Fourier Transform (IFFT) would be applied to the received filtered signal data. The resulting output of the IFFT would be the sinc function shown in Figure 2–4, centered around some time delay, t_d. The first nulls of the sinc function are located at approximately $\pm 1/f_b$ away from the time delay [3]. This entire process is one form pulse compression in radar signal processing [3]. The larger the bandwidth of the signal, the smaller the pulse width becomes in the time domain. According to [3], the benefit of performing an FMCW sweep is, "...the echo from a single point scatter concentrates most of its energy in a very short duration, thus providing good range resolution while still allowing the high transmitted energy of a long pulse." This is true for FSCW radar operation as well. Comparing the main lobe of Figure 2–4 to Figure 2–3, Figure 2–5, or Figure 2–6, it can be seen that Figure 2–4 has a shorter time duration, showing that the pulse has been compressed.

As mentioned earlier, FSCW radar is the discretized version of an FMCW radar. Stepping in

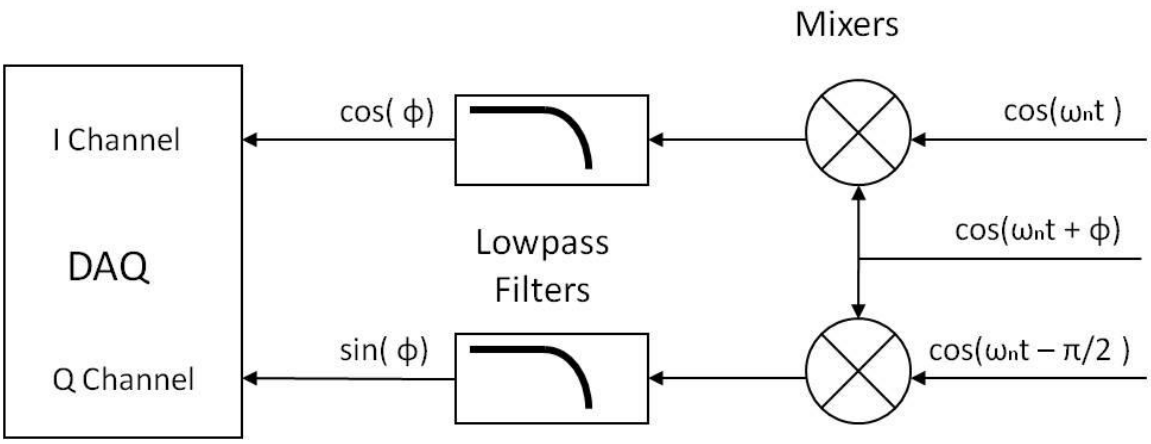

Figure 2–8: Block diagram of a radar system that has both an I and Q channel.

frequency over a specified bandwidth does offer the same results as the analog version. What is different with an FSCW radar system is the block diagram of the radar system. In Figure 2–2, there was only one channel going into the frequency counter. However, looking at Figure 2–8, there are two channels going into the data acquisition device (DAQ), the I (in-phase) and Q (quadrature) channels. The benefit of having both an I and Q channel is it allows for the complete phase recovery of the return signal by sampling the amplitudes of the incoming signals.

When the radar system is sampling the phase of the received signal it is really recovering the complex exponential of the traveling electromagnetic wave. The electric field of a signal propagating in free space in the z-direction only is

$$\bar{E}(z) = \bar{a}_y E_0 e^{-j\beta z} \tag{2}$$

where E_0 is the electric field intensity, and β is the propagation constant [5].

The transformation of the complex exponential using Euler's Identity is

$$E_0 e^{-j\beta z} = E_0(\cos\beta z - j\sin\beta z)\ . \tag{3}$$

Another way of looking at Equation (3) is there is a real part and an imaginary part. The only difference between the sine and cosine terms is a ninety (90) degree phase shift between each other. This relationship is,

$$\sin(\beta z) = \cos(\beta z - \tfrac{\pi}{2})\ . \tag{4}$$

Figure 2–8 shows what the I and Q channels represent. The I (in-phase) channel represents the real part of the traveling EM wave at the measurement point z while the Q (quadrature) channel represents the imaginary part of the traveling EM wave:

$$I_{Channel} = E_0 \cos \beta z \quad (5)$$

$$Q_{Channel} = E_0 \sin \beta z \, . \quad (6)$$

After the DAQ has recorded the amplitude values of the I and Q channel for the different frequencies, it must be processed with a computer compression algorithm [6]. The complex phasor of the signal is,

$$Complex\ Phasor = I_{channel} + jQ_{Channel} \quad (7)$$

This is performed at each discrete frequency over the operating bandwidth.

The next step in transforming the complex phasor information to a time delay mathematically is a little more complex. It requires the application of the inverse Fourier transform (IFT). However, the IFT can only be used on continuous-time variables. So, the inverse fast-Fourier transform (IFFT) is used for transforming the complex phasor information [6]. The basic algorithm for transforming the complex phasor information to the time domain is

$$Recovered\ Time\ Signal = IFFT[Complex\ Phasor] \quad (8)$$

Those two algorithms are the fundamental operations for transforming complex phasor information to the time domain.

Figure 2–9 and Figure 2–10 give a graphical representation of how the phase is sampled in the frequency domain and transformed back to the time domain to recover the time delay of the target. These graphs are a visual representation of a Fourier transform pair such as an impulse function given here:

$$\delta(t - t_d) \quad <=> \quad e^{-j2\pi f t_d} \, , \quad (9)$$

where t_d is the time delay of a return signal and f is the continuous variable for frequency. Equations (2) through (8) represent the entire process summed up in the transform pair given in equation (9). The radar operating in FSCW mode is sampling the phase information in the frequency domain to recover the delay of the time domain pulse.

The time base (x-axis) for Figure 2–10 is reconstructed from the total number of sample points and the frequency step of the stepped-frequency radar [3]. The time step is

$$T_s = {}^{1}/_{K\Delta f} \quad (10)$$

where K is the total number of samples and Δf is the frequency step. The range to the target is generally of more interest than the time delay of the receive signal. The conversion to range is

$$\Delta R = \frac{cT_s}{2} = \frac{c}{2K\Delta f}, \quad (11)$$

where c is the speed of light in a vacuum and ΔR is the range step between the samples. The

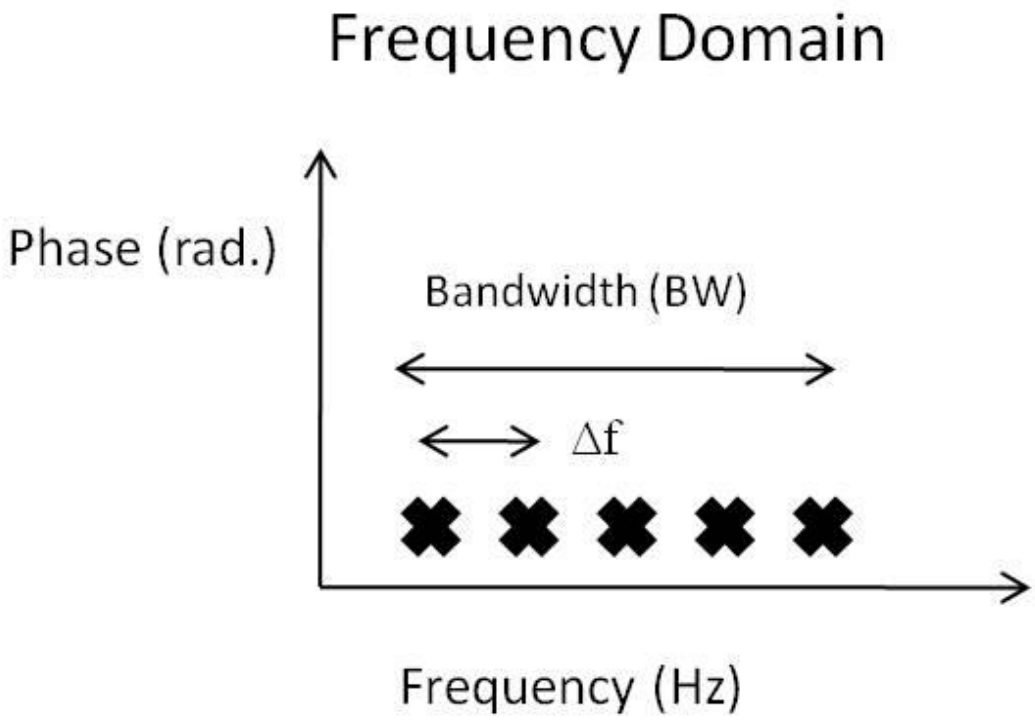

Figure 2–9: Plot showing the sampling of the phase information in the frequency domain.

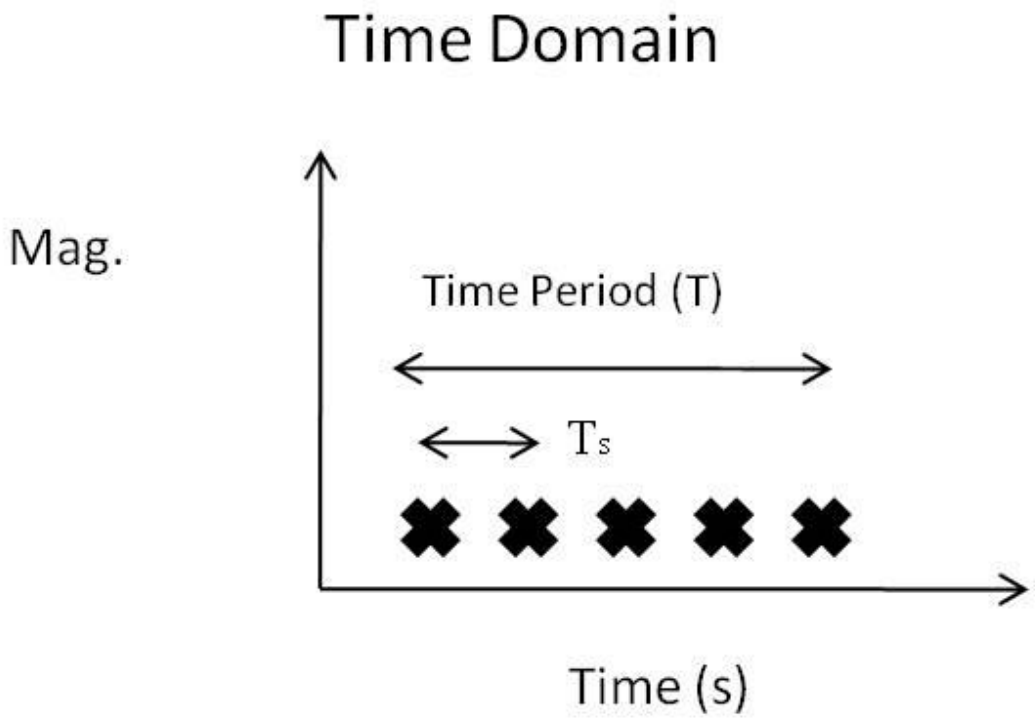

Figure 2–10: Plot showing the transformation of the phase data back into the time domain.

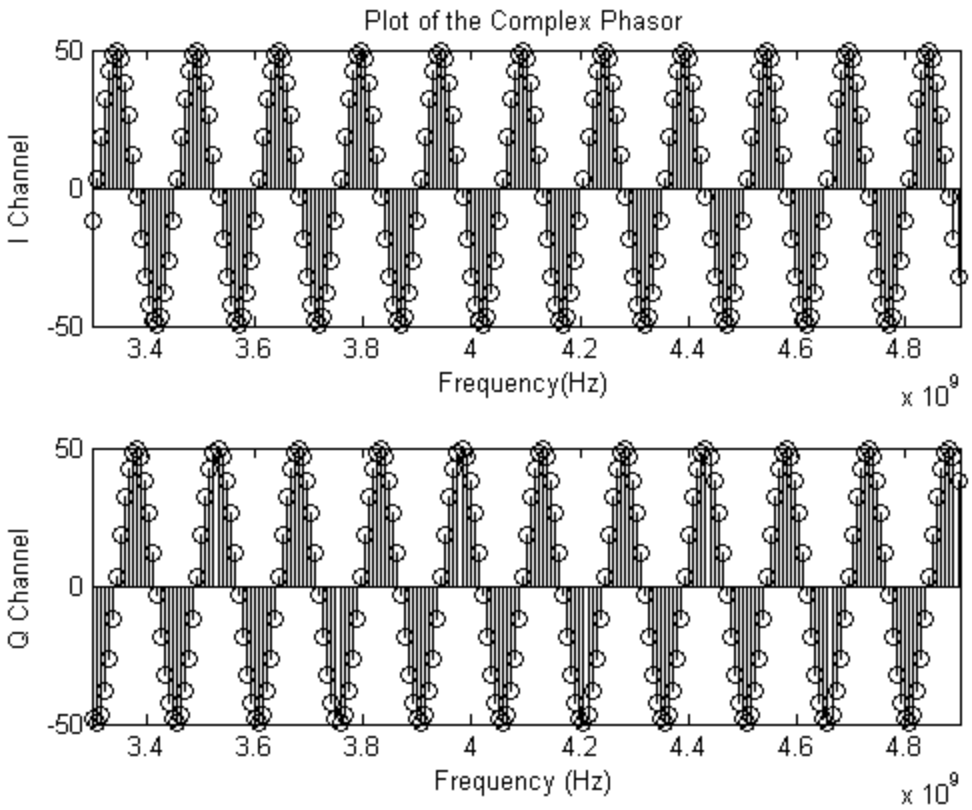

Figure 2–11: Stem plot using MATLAB of the real and imaginary amplitude values.

factor of 2 results because of the total round trip of the received signal is twice the distance to the target. Also, ΔR represents the range resolution of the radar system since T_s represents the time domain width of the compressed pulse.

Again referring to equations (10) and (11), it is possible to specify the bandwidth, $K\Delta f$, of the signal by changing the number of samples, K. However, this would affect the range resolution of the recovered pulse since bandwidth and range resolution are inversely proportional. Another aspect that the radar operator can specify is the maximum range the radar can measure before time aliasing occurred. Assuming that the bandwidth stayed the same by decreasing the frequency step, the maximum range could be increased by increasing the number of sample points.

Figure 2–11 shows a plot of the complex phasor considered in equations (3) through (6). The plots were generated using the MATLAB script found in Appendix A. Notice how the real and imaginary plots are separated from each other by a ninety (90) degree phase shift. When one plot is at its maximum the other is zero. Also, note that the x-axis units are in Hertz. This is because the propagation constant, β, is a function of frequency:

$$\beta = \frac{2\pi f_n}{c}, \tag{12}$$

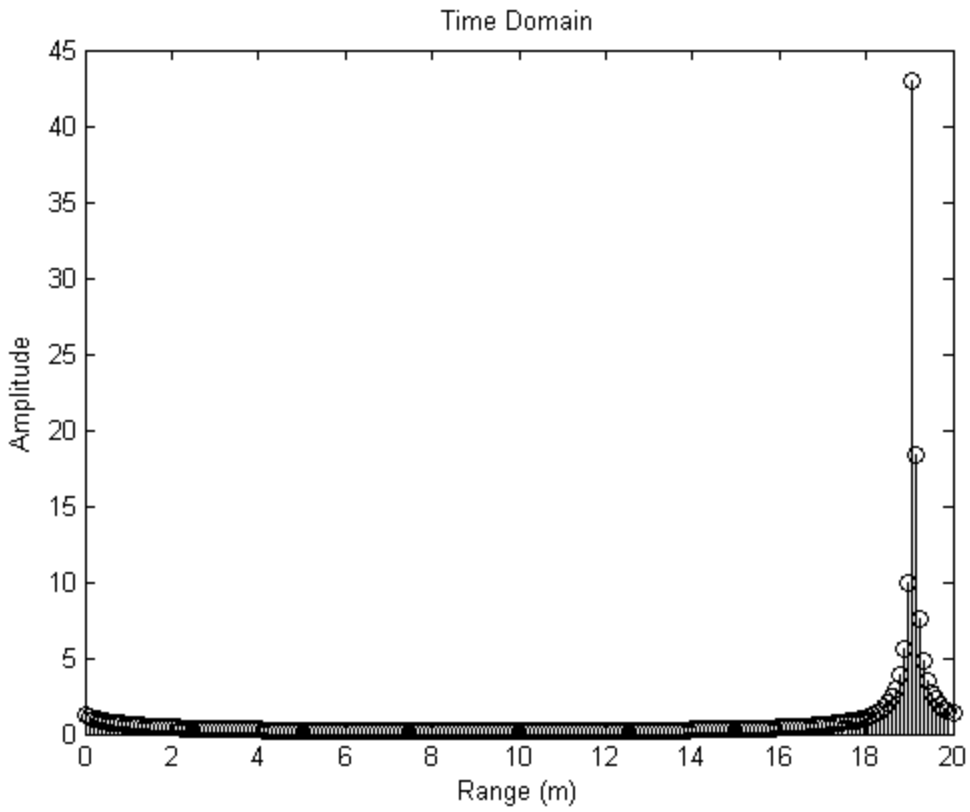

Figure 2–12: Stem plot using MATLAB showing the time domain plot of a single target at 19 m.

where f_n is the stepped frequency in Hertz (Hz) and c is the speed of light in a vacuum. When the radar is in FSCW operation, the phase of the received signal is the propagation constant proportional to that specific frequency.

Figure 2–12 shows the IFFT for the complex phasor data shown in Figure 2–11. Note that Figure 2–12 is the discretized version of Figure 2–4. Also, the shape of Figure 2–12 resembles that of a sinc function. The code for generating Figure 2–12 can be found in Appendix A. By comparing those two graphs, it can be seen that taking the IFFT of the complex phasor data not only compresses the pulse data, but it performs the matched filtering as well. This is how the data collected from the VNA will be processed and displayed. The real and imaginary data will be measured and recorded. Then the data is processed using a MATLAB script program that implements equations (7) through (10) allowing for the recovery of the range of all of the targets.

REFERENCES

[1] Merrill I. Skolnik, *Introduction to Radar Systems,* McGraw-Hill, 2001

[2] Peyton Z. Peebles, Jr., *Radar Principles*, John Wiley and Sons, 1998.

[3] Mark A. Richards, *Fundamentals of Radar Signal Processing*, McGraw-Hill, 2005.

[4] Bernard Sklar, *Digital Communications: Fundamentals and Applications,* Prentice Hall, 2006, pp. 122-124.

[5] David K. Cheng, *Field And Wave Electromagnetics,* Addision-Wesley, 1983, pp. 298-301.

[6] Merril Skolnik, 2nd ed., *Radar Handbook,* McGraw-Hill, 1990.

CHAPTER 3

SYSTEM SETUP AND MEASUREMENT VALIDATION PROCEDURES

As mentioned in the introduction, the process implemented for detecting a target in an enclosed room is using a variable delay between the current pulse and the reference pulse as a single stage canceller MTI filter. The room measurements were taken in a hallway at Oklahoma State University's University Multispectral Laboratories (OSU-UML) at the Richmond Hill Research Center just north of Stillwater, Oklahoma. Prior to the hallway measurements, a series of tests were run to confirm the operation of the radar system.

The HP 8753ES Vector Network Analyzer (VNA) was used as the radar system. The VNA was set up as a bistatic radar with port 1 being the transmitter and port 2 being the receiver. The operating frequency range was from 3.3 to 4.9 GHz with a total of 1601 data points taken. The sweep time of the VNA was set to 1 second to provide enough dwell time on each frequency. The power level was set to 10 dBm (10 mW). Before using the VNA as a radar system, it was calibrated over the specified frequency range. Calibrating the VNA removed any amplitude distortions that are typically associated with a linear FSCW radar system [1].

There were four different measurement scenarios tested to ensure the radar system was operating as intended. The first two scenarios involved the antennas pointing directly at each other and a six foot cable connected between the transmit and receive ports. The antenna test determined the time delay of the antenna systems and feed network to account for any discrepancies in the measured range of actual targets. The six foot cable delay test provided a known length to test range measurement accuracy of the radar system. Both tests also provided a simple test to ensure the signal processing algorithms were coded properly. Next, the radar was operated in an anechoic chamber environment. The anechoic chamber used was the ETS-Lindgren SMART 10 with a six meter quite zone. Operating the radar in the anechoic chamber provided a low clutter environment and another way to prove the operation of the radar system. The antenna delay, cable delay, and anechoic chamber tests provided a way to first test the radar in a simpler environment to prove the operation of the radar. Lastly, the radar was tested in a hallway without any targets present. The system coherency of the radar and

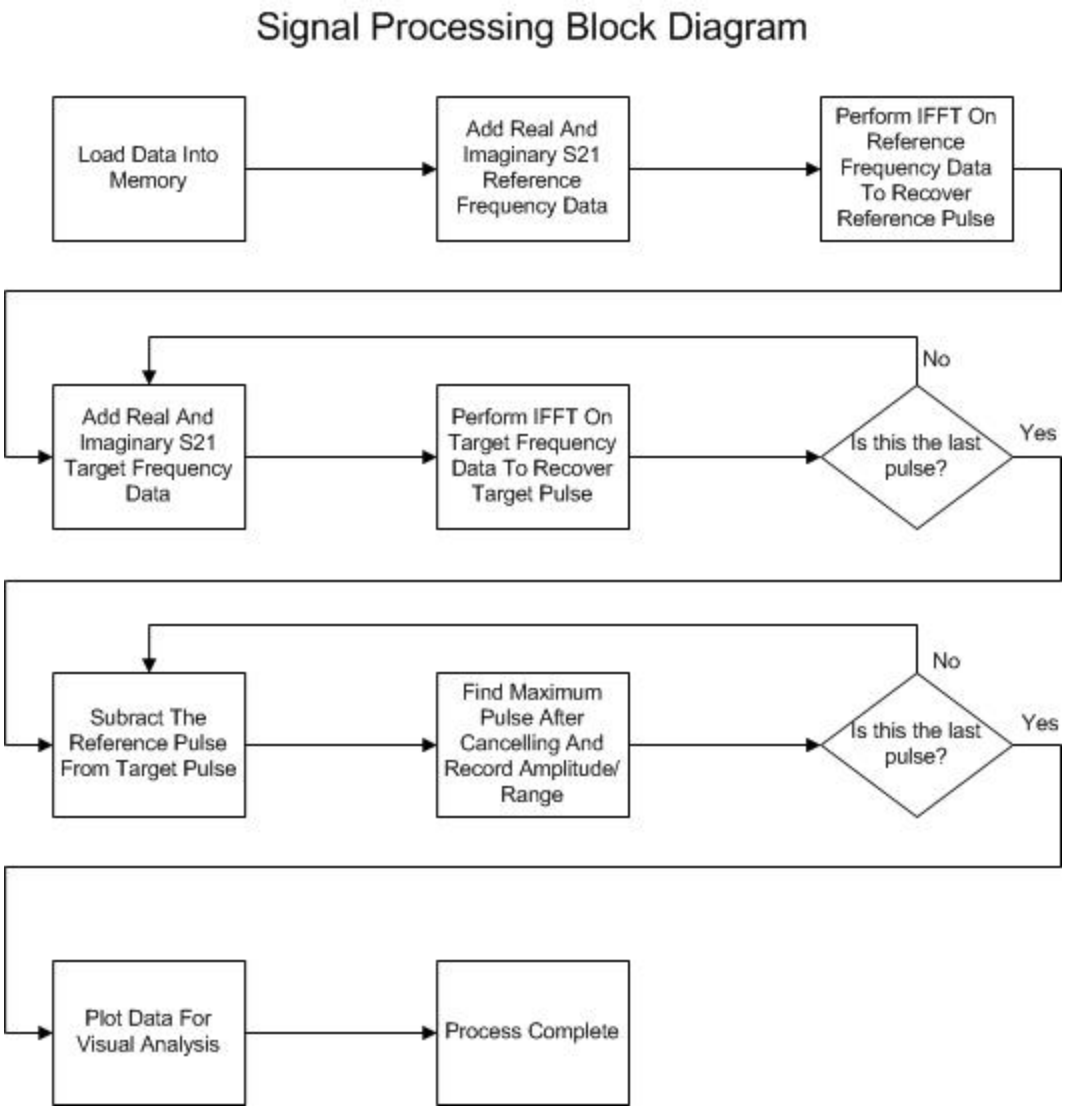

Figure 3–1: Signal processing block diagram for locating targets buried in clutter.

hallway was tested to ensure that the reference pulse had a long enough channel coherence time. Using the hallway also provided a realistic environment similar to the one that under which the radar is ultimately intended to operate. In the proof of concept demonstration, the corner reflector, the sphere, and a human subject will be used as targets in the hallway.

SYSTEM MEASUREMENT VALIDATION

A signal processing routine was established to extract the targets from the measured step-frequency returns. Figure 3–1 shows the signal processing block diagram. As discussed in Chapter 2, the separate in-phase and quadrature data was converted into a single complex

number data set. Then, the IFFT was applied to yield the range-resolved returns. The reference pulse was then subtracted from subsequent pulses thus applying a single-stage MTI filter. The maximum pulse value in the cancellation data was then found and the range and amplitude of that value was recorded. After all of the pulses were processed, the range-resolved return signals, the results after MTI cancellation, and the location of the range and amplitude for the maximum pulse were all plotted for visual inspection.

As mentioned in the introduction, the antenna delay of both transmit and receive antennas were measured to ensure proper operation of the radar system. This data was collected by pointing the two antennas directly at each other with no gap in between. During the calibration process of the VNA, the feed network including cables, adaptors, and connectors were calibrated out of the system. However, the antennas could not be calibrated directly out of the system. The delay of the antennas had to be measured. After measuring the antenna delay, a six foot cable was connected between the transmit and receive ports. As mentioned earlier, this test determined the range measurement accuracy of the radar system. Both tests also provided an opportunity to test the radar system operation before taking additional measurements requiring more time and effort. Figure 3–2 and Figure 3–4 show the plots of the complex phasor data of the antenna and six foot cable delays. Notice that Figure 3–2 and Figure 3–4 look very similar to Figure 2–11. They are not exact because frequency responses of the two antennas and six foot cable are not flat across the entire operating band. Also, Figure 2–11 is an idealized model with no noise present. Figure 3–3 and Figure 3–5 show the recovered time domain pulse of the both antenna's combined delay and the delay of the cable. Again, there is a close similarity between Figure 3–3 and Figure 3–5 and Figure 2–12. Figure 3–2, Figure 3–3, Figure 3–4, and Figure 3–5 show and verify the operation of the radar system, including, the IFFT processing. The MTI signal processing has not been verified at this point.

Testing the radar system in the anechoic chamber provided a testing procedure to establish the noise floor of the radar system. It also allowed for the testing of the MTI signal processing routines. The targets used in this test were a corner reflector for large RCS and a sphere for small RCS. Since this chamber was a full anechoic chamber, there were RF absorbing cones placed on the entire floor. This prevented any target from being moved from one range bin location to another. Instead, a reference pulse was first measured with no targets present. Then each target was placed in the chamber and their S21 frequency data was measured. Typically this anechoic chamber was used to make antenna pattern measurements. Therefore, the chamber had two large metal pylons that jutted out from the floor that were used to mount test antennas. No matter which side of the chamber was chosen for the location of the targets, a pylon would always appear in the pulse data. This provided an opportunity to see if the pylon returns could be cancelled by MTI processing.

Figure 3–6 shows the reference pulse with no target present inside the anechoic chamber. There were two main strong backscatter locations in the chamber. The first was the pylon in the anechoic chamber at approximately 30 foot range while the second was the wall behind the pylon at approximately 38 feet. All amplitude information beyond the back wall is considered

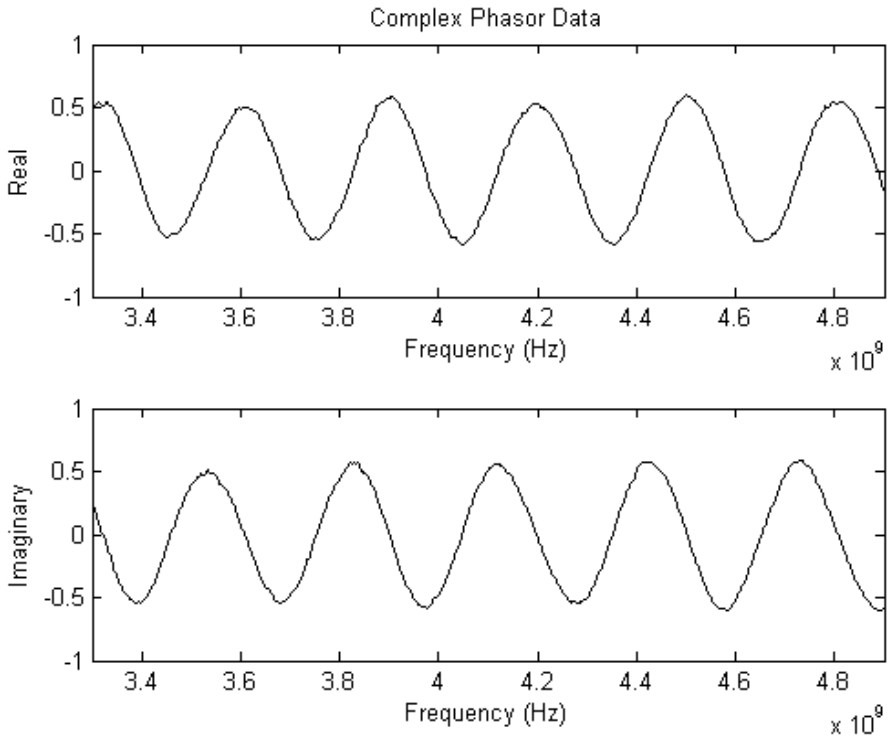

Figure 3–2: The complex phasor data of the antenna delay measurements.

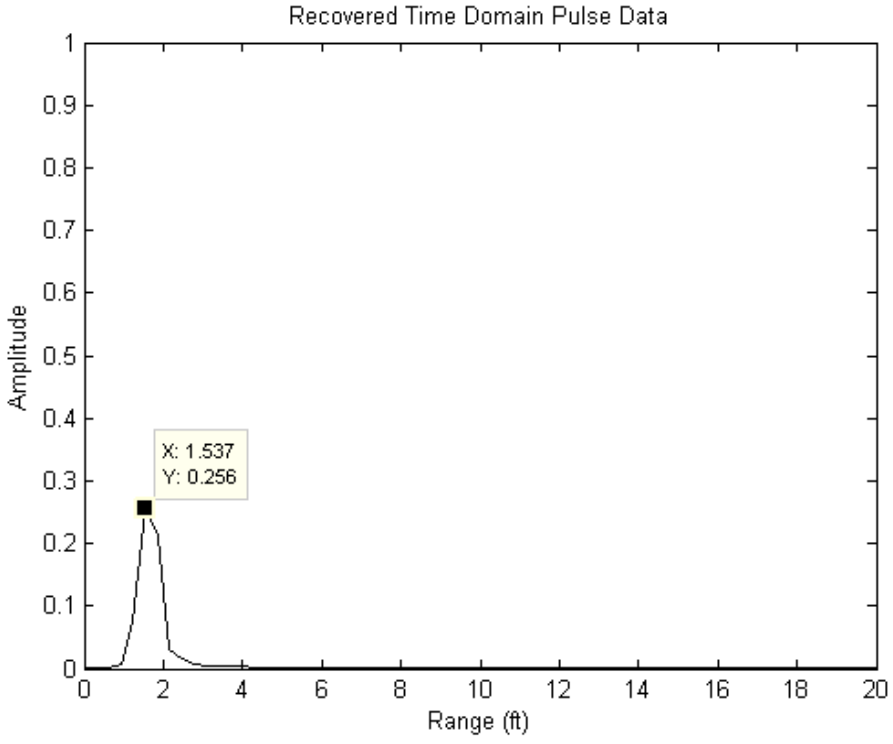

Figure 3–3: The recovered time domain pulse data of the antenna delay measurements.

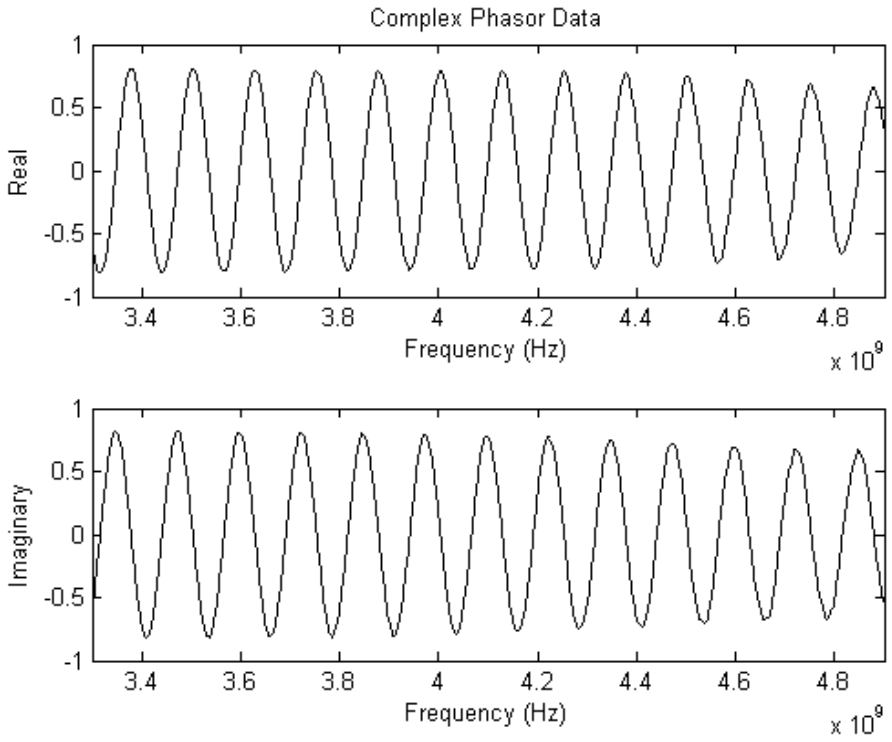

Figure 3–4: The complex phasor data of the six foot cable with a phase velocity of 0.66.

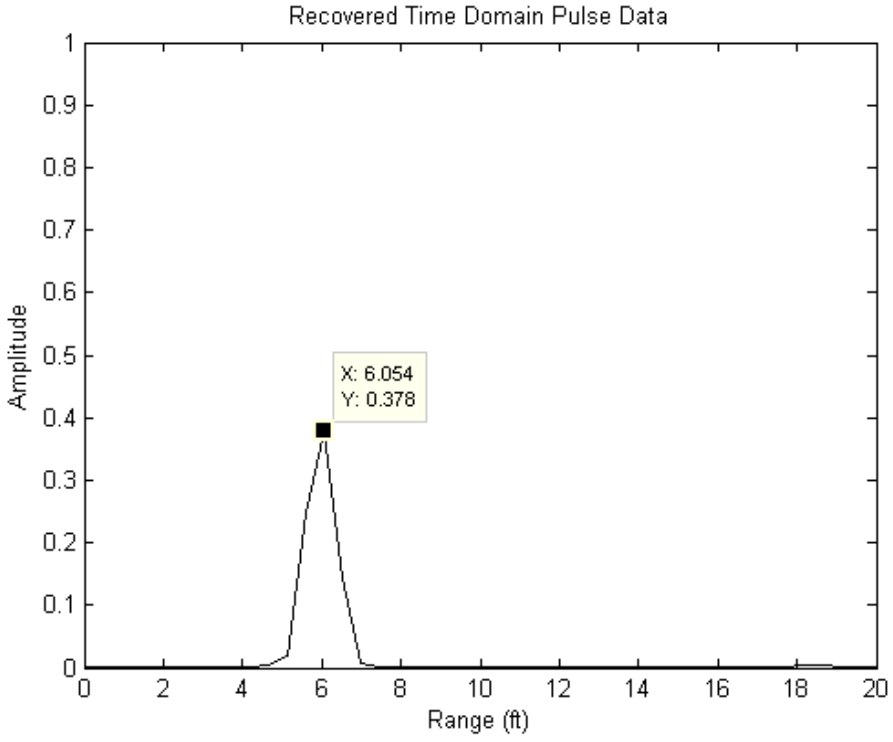

Figure 3–5: The recovered time domain pulse of the six foot cable delay measurement.

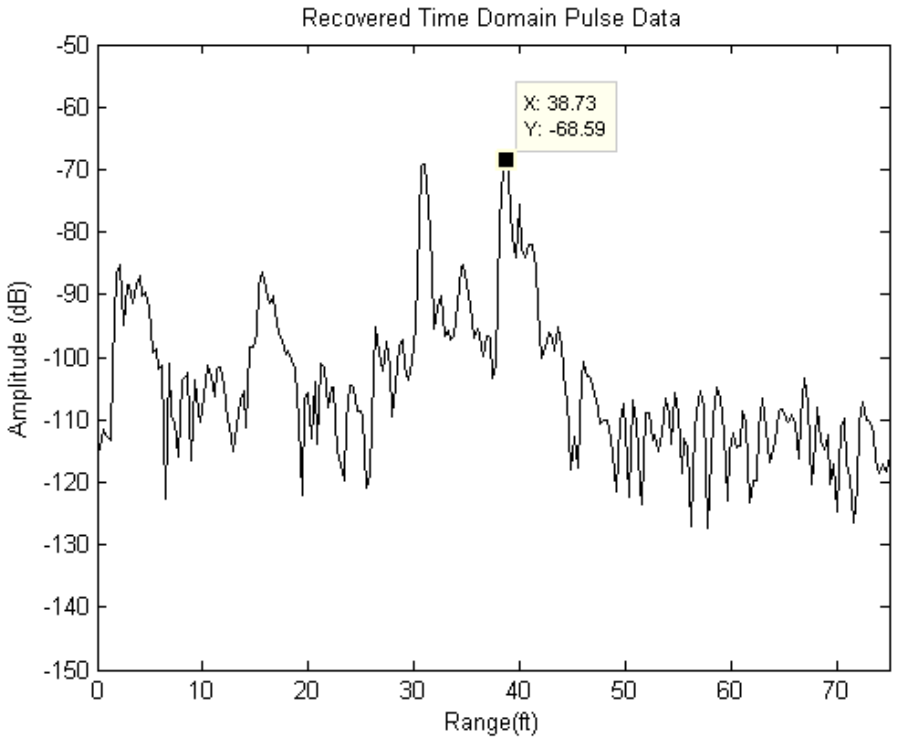

Figure 3–6: The return reference pulse inside the anechoic chamber.

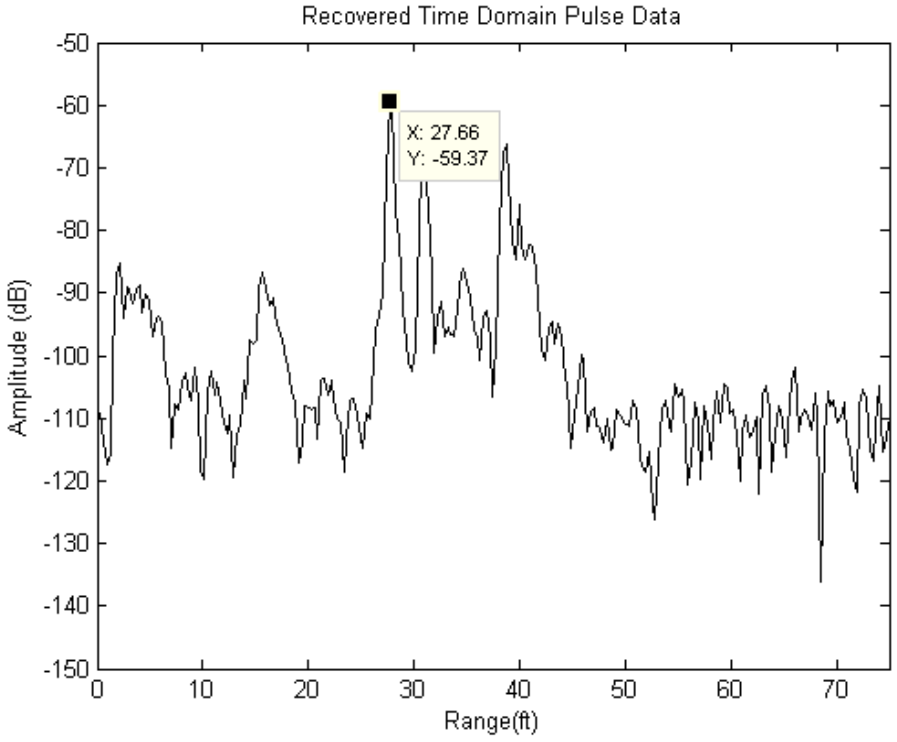

Figure 3–7: The return pulse inside the anechoic chamber with the corner reflector present.

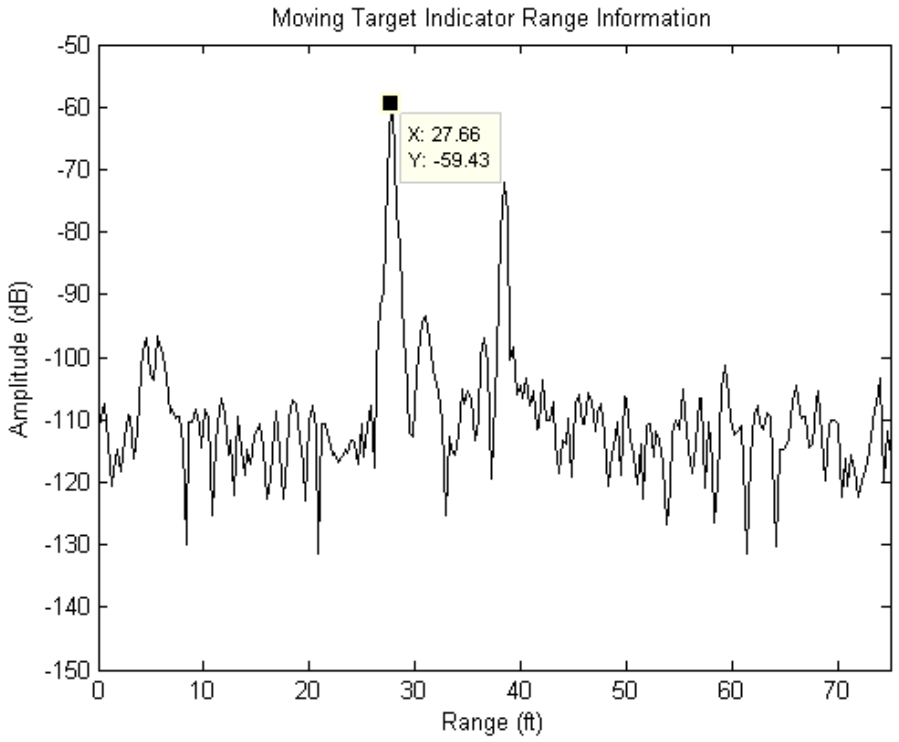

Figure 3–8: The corner reflector returns after MTI cancellation in the anechoic chamber.

the noise floor of the system. Figure 3–7 shows the recovered pulse of the corner reflector inside the anechoic chamber located at approximately 27 feet. The pylon and the back wall can still be seen in the range information, but the amplitudes of them both are smaller than the corner reflector returns. Figure 3–8 shows the cancellation plot between the reference pulse without the corner reflector and the second pulse with the target. The back wall return is partly suppressed after cancellation, but is still visible. Its magnitude is much less than the corner reflector returns. The pylon was suppressed by approximately 25 dB after MTI cancellation, indicating much better suppression than the back wall.

After the testing was done with the corner reflector, a 14-inch diameter conducting sphere was placed in the chamber on top of a large Styrofoam block. At the operating frequencies of the radar, the index of refraction of Styrofoam is approximately one, giving minimal reflection. The sphere therefore appears to the radar to be in free space. Figure 3–6 was also used as the reference pulse for locating the sphere inside the anechoic chamber. Looking at Figure 3–9, the backscatter from the sphere was much lower than the anechoic chamber wall reflection. A marker was added to the return pulse of the pylon to distinguish between the sphere and the pylon. Figure 3–10 shows the returns after the MTI cancellation with the reference pulse of Figure 3–6. The sphere can be seen. Note that the peak-value markers in both Figure 3–9 and Figure 3–10 are located at two different range values. Even with the sphere being relatively

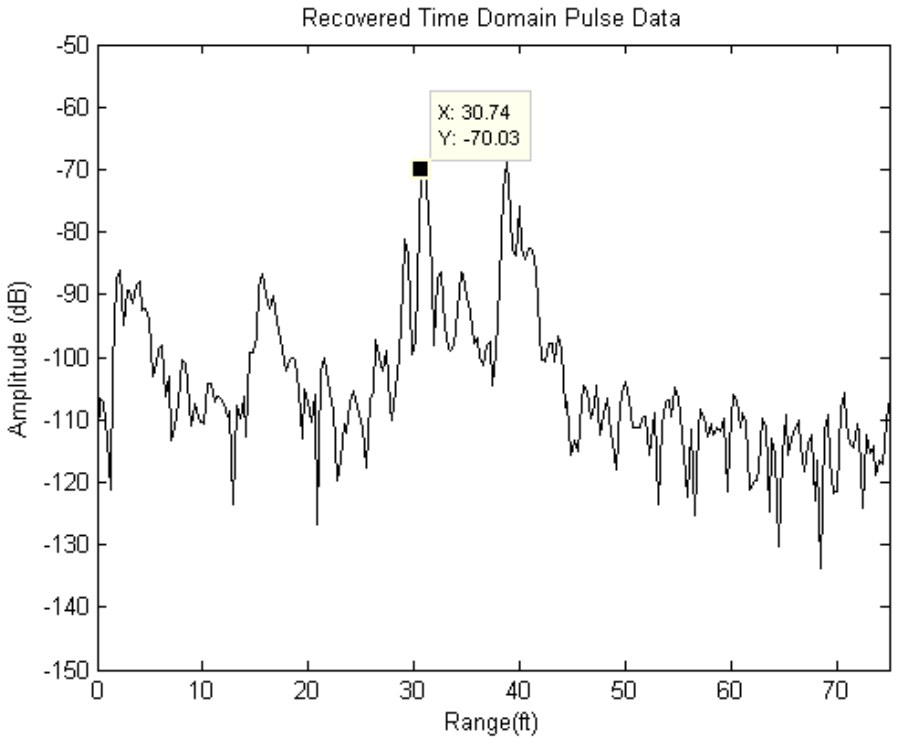

Figure 3–9: The return pulse inside the anechoic chamber with the sphere present.

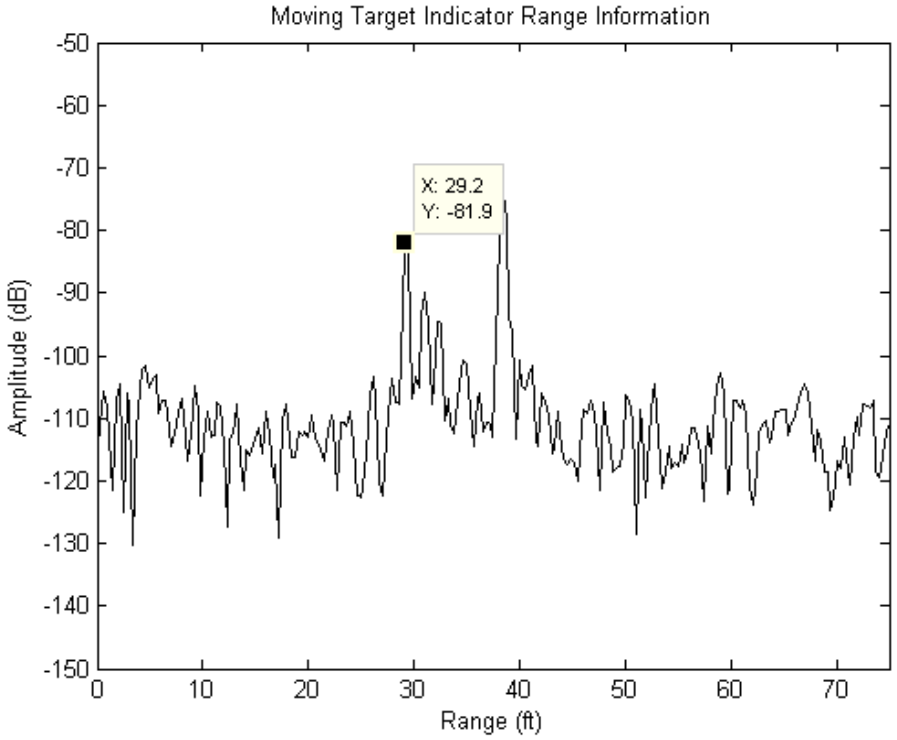

Figure 3–10: The pulse after cancellation between the reference pulse and the second pulse showing the location of the sphere.

close to the pylon in the range dimension, the radar was able to resolve the two objects using cancellation. The only problem with Figure 3–10 was the amplitude value of the sphere was smaller than the amplitude of the back wall of the anechoic chamber making it difficult to detect a target according to the block diagram in Figure 3–1. This will be discussed further in Chapter 4.

SYSTEM COHERENCY

One requirement for MTI operation of a radar system is that all channels must have strong coherence from pulse to pulse [1], [2], [3], [4]. The operation of this radar system is different than the usual MTI radar, but it too requires a coherent system. It is necessary to show that over a given time the system still remains coherent. The antenna and cable delay and anechoic tests were performed in a short time (less than 15 minutes) under highly controlled conditions. Therefore, it was not necessary to test for the coherence of the system over long time period either with the antennas pointing at each other or in the anechoic chamber. In the real world application of this radar system, it would be hidden away somewhere in a hallway continuously operating. Over time it is possible that the system response would change, due to changes such as the temperature changing in the hallway causing the walls to either expand or contract slightly or a simple system drift. The system coherency test was performed in the same hallway where the radar will be tested when trying to locate any moving targets. The entire range information is displayed on the plots to account for multipath and multiple bounces that occur in the hallway.

The coherence of the VNA was tested over an approximate two hour time interval from 9:00 at night to 11:00pm. The test was performed at this time period to ensure that no one could walk by and change something in the hallway disrupting the test. An initial measurement was taken at the beginning of the test as shown in Figure 3–11. The time lag between each pulse was fifteen minutes, except between pulse 3 and pulse 4 which was twenty minutes. The coherency of the system was tested by using the same MTI signal processing technique discussed in Figure 3–1. The initial pulse was subtracted from all other pulses, then an average amplitude value for each pulse difference was calculated. It was assumed that over time the average difference would become larger from pulse 1, indicating that the system was drifting. If the system never drifted and the environment never changed, the difference pulse would then only consist of noise from the system.

Notice the data cursor points in Figure 3–11. There is one approximately at 45 ft, one at 110 ft, and one at 230 ft. The 45 foot data cursor point represents the narrowing of the hallway. The 110 foot data cursor point represents the back wall of the hallway. Any signal returns beyond the back wall of the hallway represents multipath and multiple bounces of the transmitted signal. The third data point is either due to multipath, to multiple bounces inside the hallway, or both. These points should be remembered when looking at the difference plots. Also, notice that the noise floor for Figure 3–11 does not show up until around 300 ft which is much further

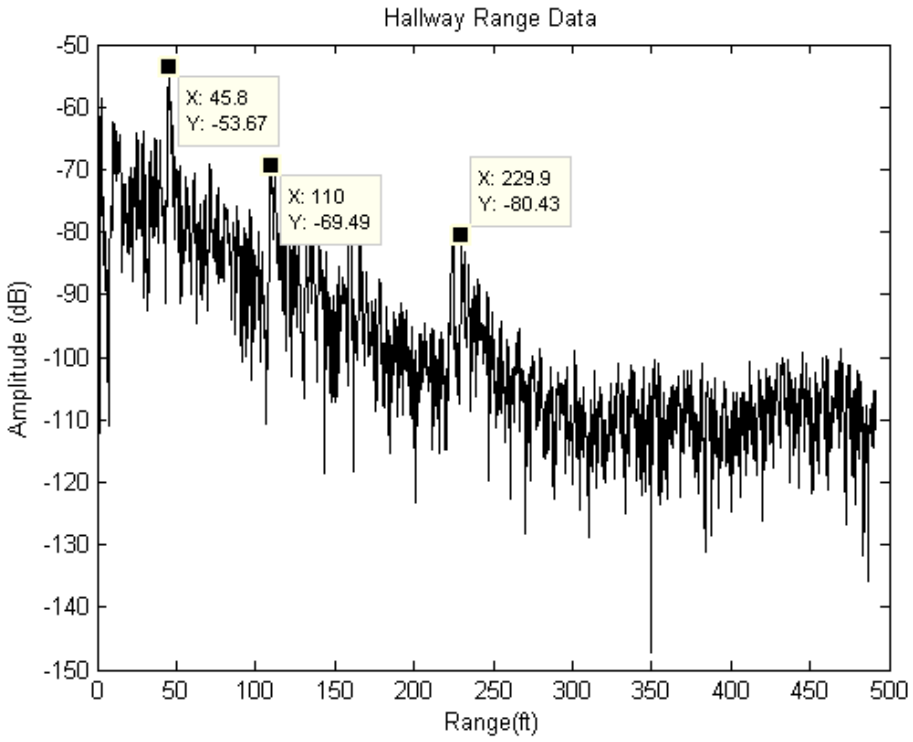

Figure 3–11: The reference pulse for the system coherency test.

in distance than inside the anechoic chamber.

Figure 3–12, Figure 3–13, and Figure 3–14 show the MTI cancelled returns with no target present at fifteen minutes, one hour, and two hour delays. The strong reflection points in Figure 3–11 are effectively cancelled even after 2 hours in Figure 3–14, indicating that even the strong reflection points are coherent. Whenever inspecting the cursor markers for the all three points, however, either those points or the surrounding data point's amplitude difference values tend to become larger over time. At the end of the two hour testing period, the 45 foot data point's amplitude grew from -95 dB to approximately -87 dB which is slightly smaller than the reflection amplitude of the sphere in the anechoic chamber.

Something that was not expected from this test was the mean amplitude value decreasing from the one hour pulse measurement to the two hour measurement. Overall, the system coherence was very high over the entire two hours, indicating that the reference pulse could be updated every fifteen minutes to two hours in this environment without loss of performance. This assumes, however, that all of the target's return signals do not fall below maximum difference amplitude. If that did happen it would make it difficult to determine if a target was present.

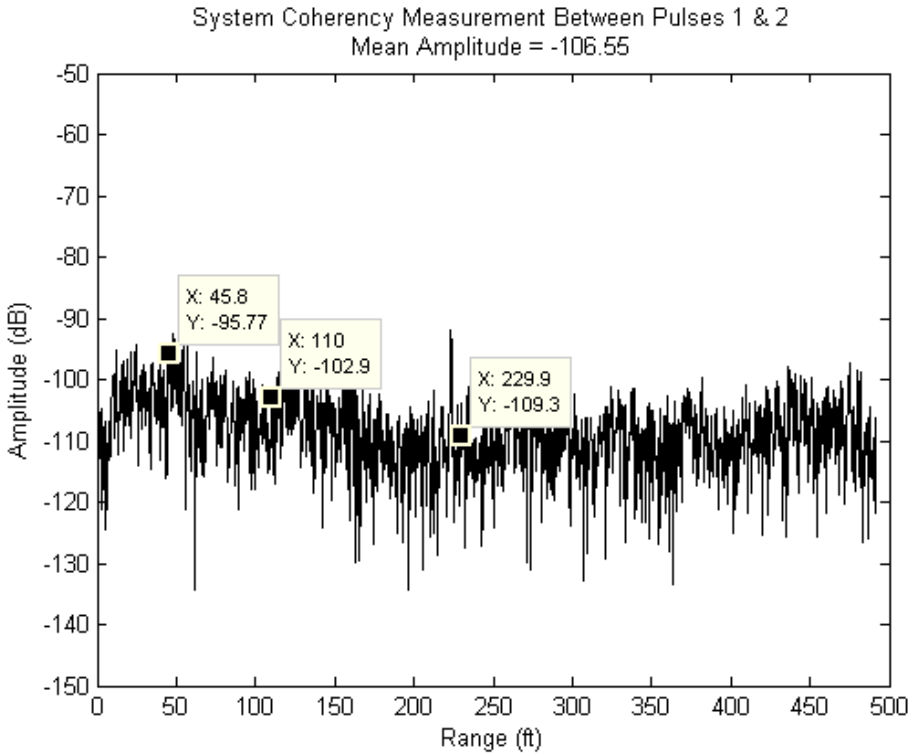

Figure 3–12: System coherency difference between pulse 1 and pulse 2 after 15 minutes has passed.

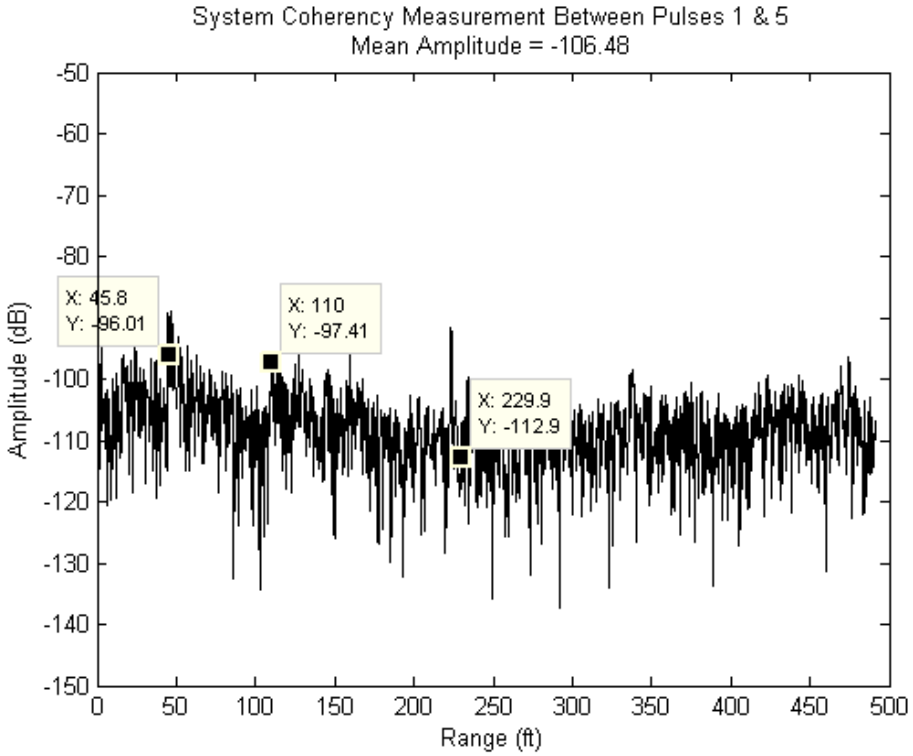

Figure 3–13: System coherency between pulse 1 and pulse 5 after an hour has passed.

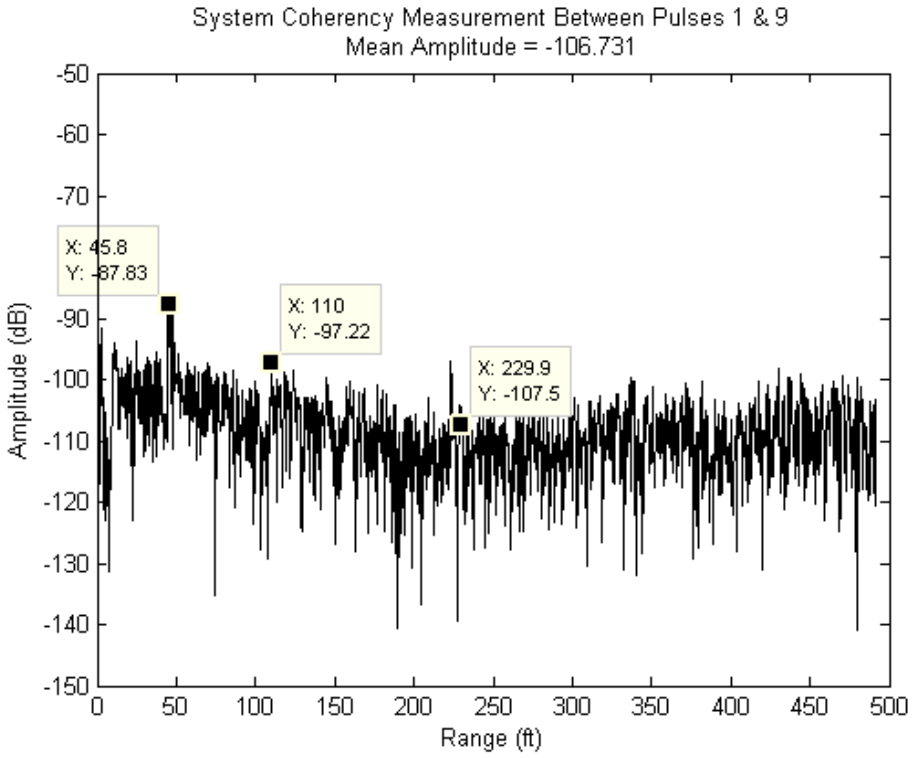

Figure 3–14: System coherency between pulse 1 and pulse 9 after two hours have passed.

REFERENCES

[1] Merril Skolnik, 2nd ed., *Radar Handbook,* McGraw-Hill, 1990.

[2] Peyton Z. Peebles, Jr., *Radar Principles*, John Wiley and Sons, 1998.

[3] Mark A. Richards, *Fundamentals of Radar Signal Processing*, McGraw-Hill, 2005.

[4] Merrill I. Skolnik, *Introduction to Radar Systems,* McGraw-Hill, 2001

CHAPTER 4

HALLWAY PERFORMANCE RESULTS

As mentioned earlier in Chapter 3, three types of targets were used in the hallway for testing the system: a corner reflector, a sphere, and a human being. For all three target cases, the test procedure was the same as in the anechoic chamber. The only difference between each target case, the data was collected on different days for each target. Therefore, it was necessary to update the reference pulse at the beginning of each test.

The dimensions for each side of the corner reflector are approximately 1 foot. The diameter of the sphere is 14 inches. The reference pulse was made without the target present in the hallway. The target was then added into the hallway starting with the second pulse. After all of the hallway data for each target was collected, the target return pulses were subtracted from the reference pulse. Then, the range of the maximum post-cancellation amplitude was found. This was done originally because the corner reflector's RCS was much higher than any reflection point in the hallway after cancellation, allowing direct identification. Because the sphere and the human subject signals were smaller than the hallway signals even after cancellation, thresholding could not be used. Increasing the power simply increased the backscatter of both the hallway and target, since the scattering process is linear.

It was shown in Chapter 3 that the entire signal processing routine used for detecting a target was effective in the anechoic chamber. After MTI cancellation, the target would appear distinctly in the returns. However, the back wall of the anechoic chamber always appeared after MTI cancellation. This too was a problem in the hallway. Not only did the back wall show up in the cancellation data, but where the hallway narrowed also appeared in the cancellation data. Originally, it was thought that those two locations appear in the cancellation data since the system did not maintain strong coherence. However, that was not the case once the system coherency was tested. This will be discussed later.

Figure 4–3 shows the radar placed at the end of the hallway. The radar was located on the west end of the hallway with both antennas pointing eastward. Figure 4–1 shows a picture of the frontal view of the radar system setup. Figure 4–2 shows a picture of the hallway from the

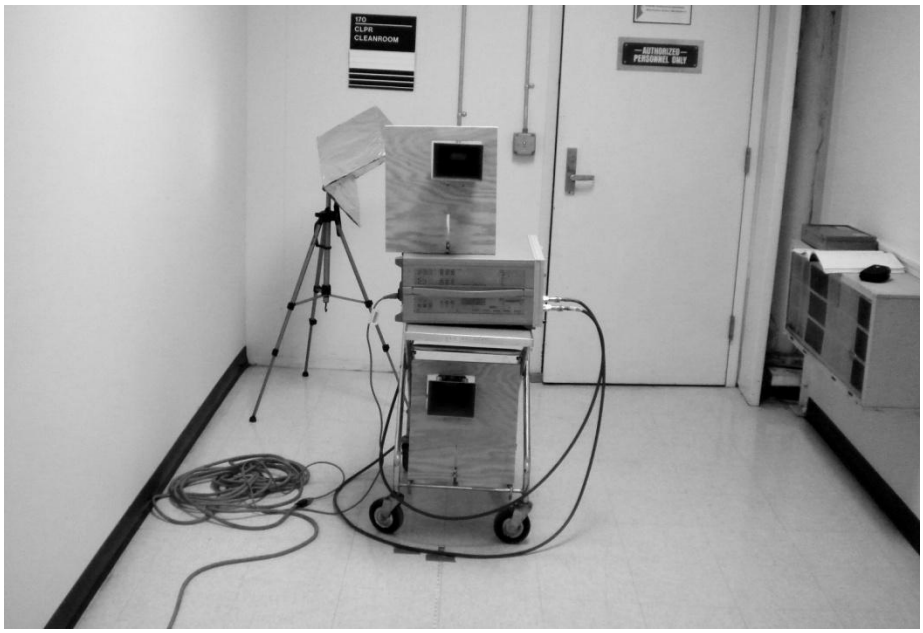

Figure 4–1: Frontal view of the radar system.

Figure 4–2: Picture of the hallway with target included.

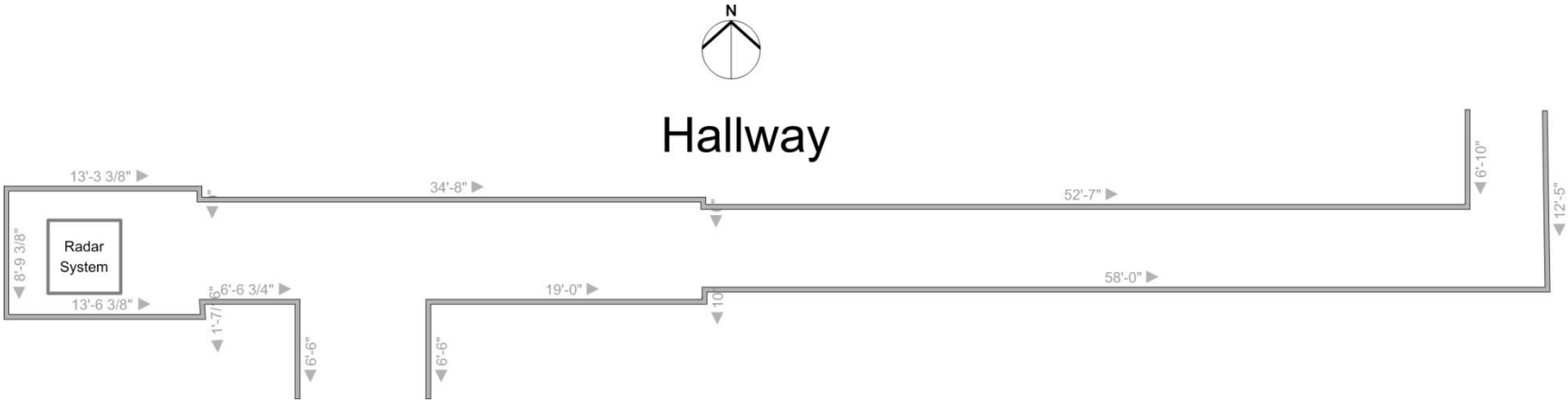

Figure 4–3: Drawing of hallway layout.

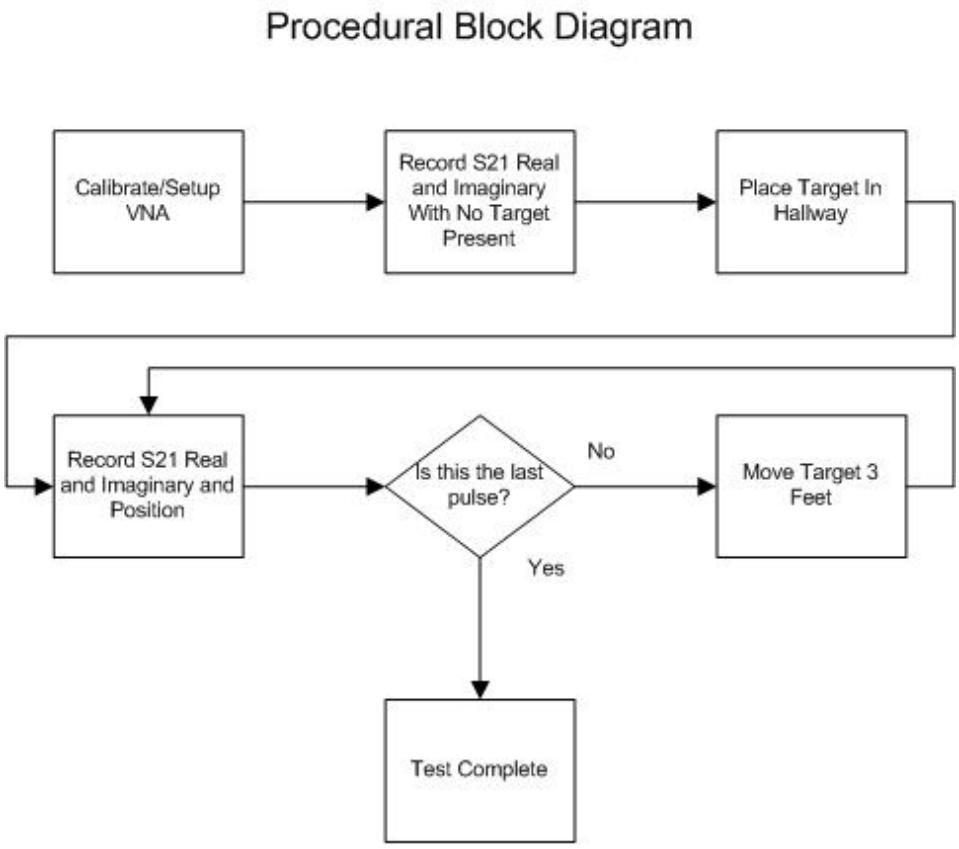

Figure 4–4: Procedural block diagram for hallway measurements.

radar's perspective, with the corner reflector placed further down the hallway. As stated earlier, measurements of the hallway's backscatter were always made before placing a target in the hallway to provide a reference pulse. The distance from the radar to the target was measured using a tape ruler for a comparison of the measured and actual range. Figure 4–4 shows the procedural block diagram for taking measurements in the hallway when a target was present. Each target was positioned at the maximum test range from the radar, and then moved forward at a discrete interval value. For all of the test cases, a total of ten or eleven pulses were taken, the first pulse being the backscatter of the hallway with no target present. As mentioned in Figure 4–4, the real and imaginary parts of the S21 parameter were saved for each pulse. The target was added at the maximum range for the second pulse. The target was then physically moved three feet toward the radar for each subsequent pulse. The different time delays between each pulse and the reference pulse is equivalent to operating the radar system with a variable PRF. As the target was moved closer, the interval between the test pulse and the reference pulse changed. Walking to the target, moving it, and walking back to the radar system required a minute or more. Well over ten minutes were needed to complete the test.

After all of the data was collected, it was then transferred to a computer for post processing. Once on the computer, MTI processing was performed as shown back in Figure 3–1. Any change

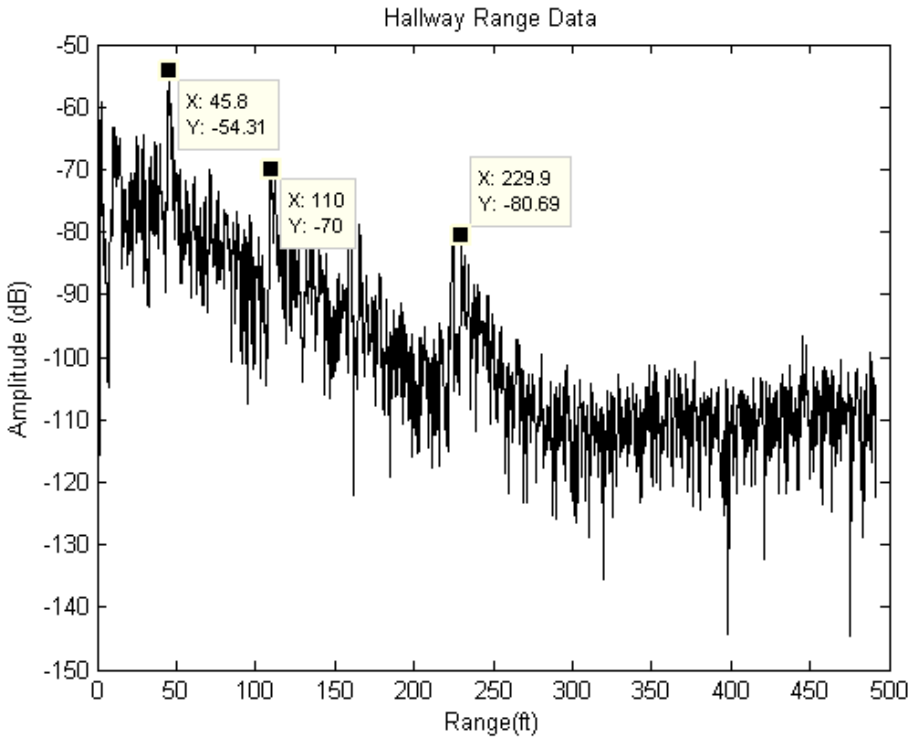

Figure 4–5: The return hallway pulse showing the strong reflection points.

in range information was recorded and plotted on a graph.

Referring back to Figure 4–3 and comparing it to Figure 4–5, a link can be drawn between the return signals of Figure 4–5 and the hallway layout shown Figure 4–3. In Figure 4–5, there are several strong reflection points that appear in the returns. The most notable one is at around the 45 foot range, corresponding to the point where the hallway narrows in Figure 4–3. There are also several other strong reflection points that show up such as the return signals before 45 ft. Most of those reflections are attributed to the narrowing of the hallway from approximately 9 ft to 8 ft, as well due to another ten foot wide hallway heading south at approximately 20 ft. Beyond 45 ft, the strongest reflection is the point around approximately 110 ft, representing the back of the hallway. As mentioned previously, reflections beyond that range are likely due to multipath or multiple bounces inside the hallway.

The 45 and 110 foot reflection points are the most problematic. Those points appear after the cancellation has been applied in Figure 4–6. This happens because either those two points appear within different range cells between pulses or energy is deflected away from the hallway returns due to the presence of the target. This is another reason for displaying the entire range data, to show the deflection of energy beyond 110 ft. In Figure 4–6, it does not appear to be a problem. The corner reflector's amplitude, at 43 ft, is much higher than those two reflection points after cancellation. However, the corner reflector is the only target whose amplitude value

is always above those two reflection points. The sphere and the human subject's amplitudes are always smaller than those two reflection points making it difficult to automatically find the range of the target. Through visual inspection and prior knowledge of the location of the targets, the sphere and the human subject can be found in the cancellation data, however.

Figure 4–5 also represents the reference pulse used for MTI processing of the corner reflector. Figure 4–7 and Figure 4–8 show the time domain plots of the second and third pulse with the presence of the corner reflector. Visually comparing Figure 4–7 and Figure 4–8 to Figure 4–5, it is difficult to determine the location of the corner reflector. After the application of MTI processing, it is visually much easier to locate the corner reflector shown in Figure 4–6 and Figure 4–9. Figure 4–10 shows the maximum amplitude for each pulse cancellation with the associated range. Figure 4–11 is the comparison plot of the actual range versus the measured range from the radar system. Put side by side, the range information in Figure 4–10 and Figure 4–11 match well, indicating that the RCS of the corner reflector is larger than the hallways after cancellation. The discrepancy in Figure 4–11 between the two ranges is the result of the system delay.

Figure 4–12 shows the time domain plot of the hallway backscatter without the presence of the sphere. Figure 4–13 and Figure 4–14 show the time domain plot of the hallway backscatter with the presence of the sphere. As with the corner reflector, it is difficult to determine the location of the sphere without having prior knowledge of its location. Figure 4–15 and Figure 4–16 are plots of pulses two and three after MTI processing has been performed. Again, the actual location of the sphere is not easily spotted without having prior information of its position despite the MTI processing. In the case of the corner reflector, its magnitude was always the largest amplitude value after MTI cancellation making it easy to identify. With the sphere, however, its magnitude is not the largest in Figure 4–15 and Figure 4–16. Figure 4–17 and Figure 4–18 also show that the sphere's return signal is smaller than the walls; the back wall and the narrowing of the hallway are identified as the strongest signals.

Figure 4–19 shows the reference pulse of the hallway clutter without the presence of the human subject. Figure 4–20 and Figure 4–21 show pulse two and three of the hallway backscatter with the presence of the human subject. As expected, it is difficult to determine the presence or the location of the human being in Figure 4–20 and Figure 4–21. Figure 4–22 and Figure 4–23 show the human returns after cancellation. It is easier to distinguish the human subject from the background in these cases. As with the sphere, the human target pulse amplitude is smaller than some of the background clutter that shows up in the processed MTI pulse data. Again, if there was no prior information about the approximate location of the human, it would be unlikely that the position of the target could be accurately identified. Figure 4–24 and Figure 4–25 also indicate that the hallway backscatter is still larger than the human target after MTI cancellation. There is only one pulse where the human subjects return signal is larger than the residual hallway returns. What was important was the returns did change with the target present, indicating that the presence of a target can be identified even if the exact location is not found.

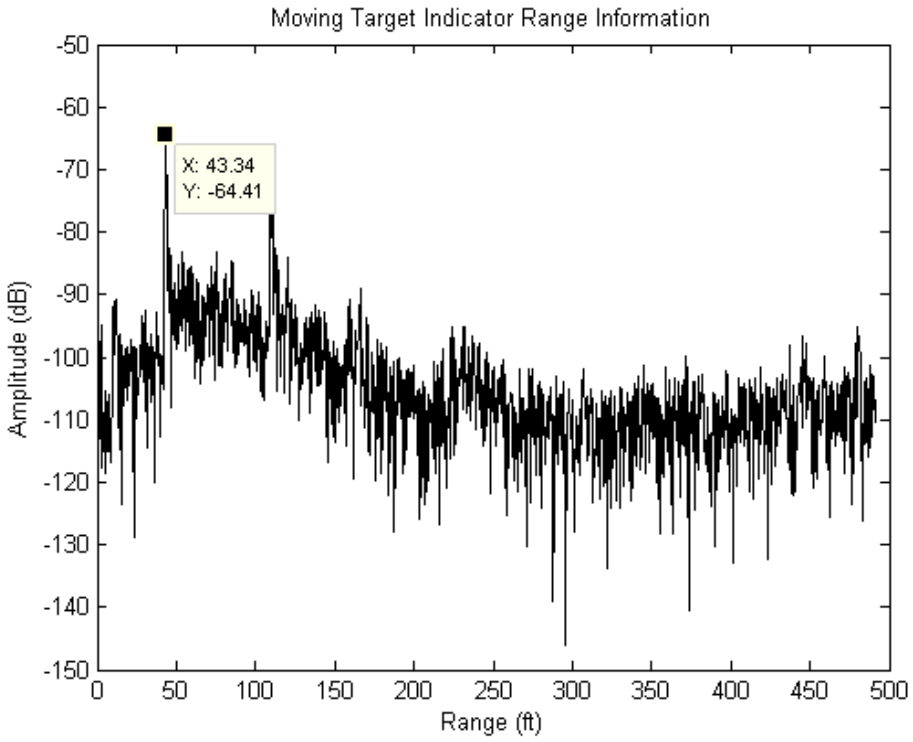

Figure 4–6: The pulse difference between pulse two and the reference pulse showing the presence of the corner reflector.

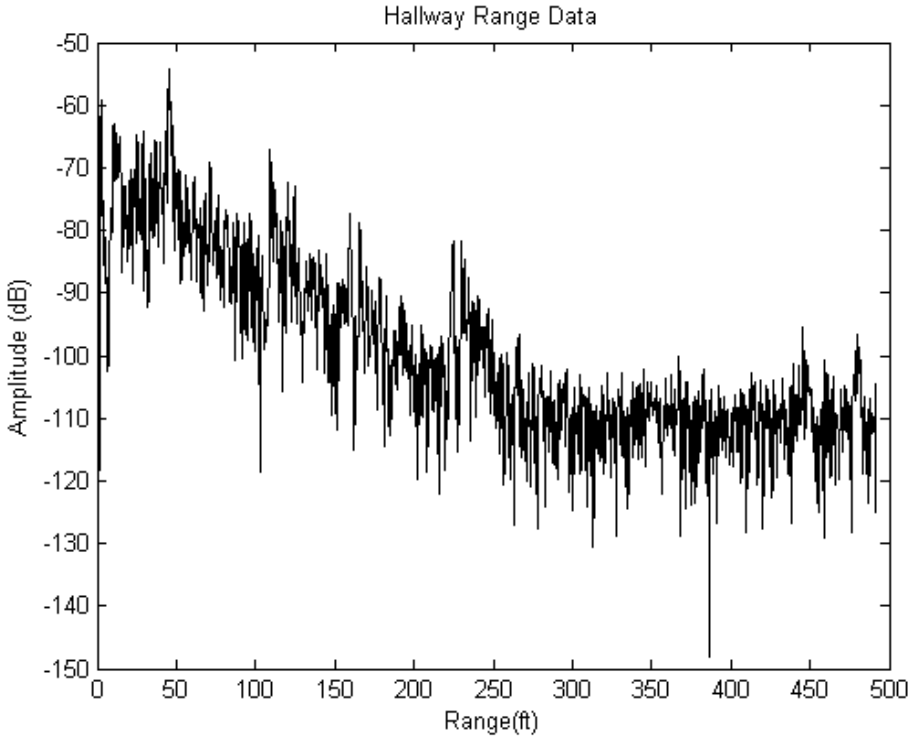

Figure 4–7: The second pulse of the hallway with the presence of the corner reflector.

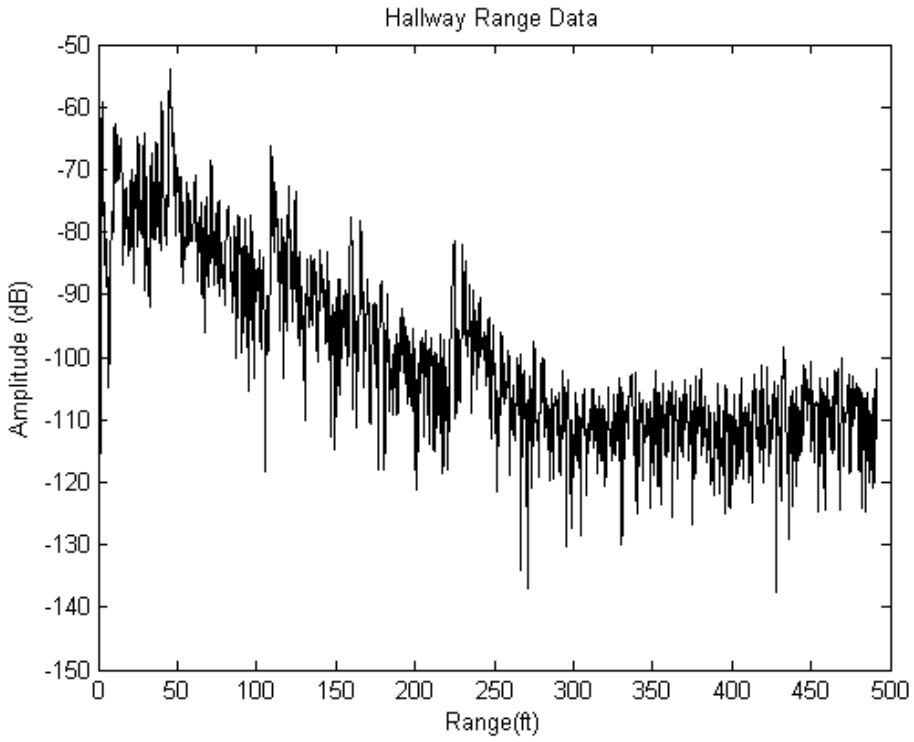

Figure 4–8: The third pulse of the hallway with the presence of the corner reflector.

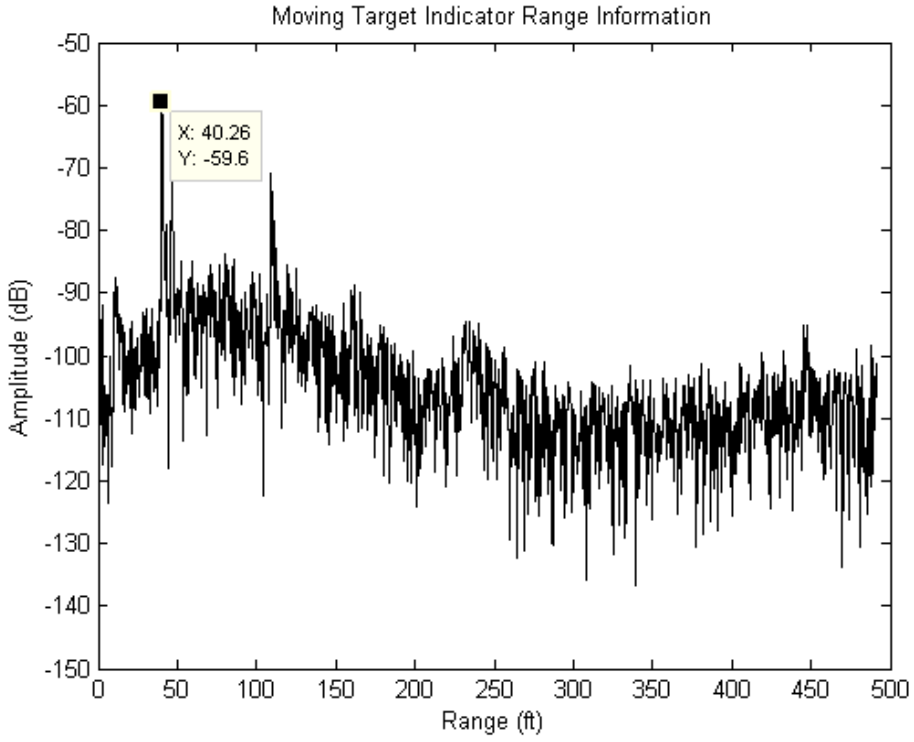

Figure 4–9: The pulse difference between pulse three and the reference pulse showing the presence of the corner reflector.

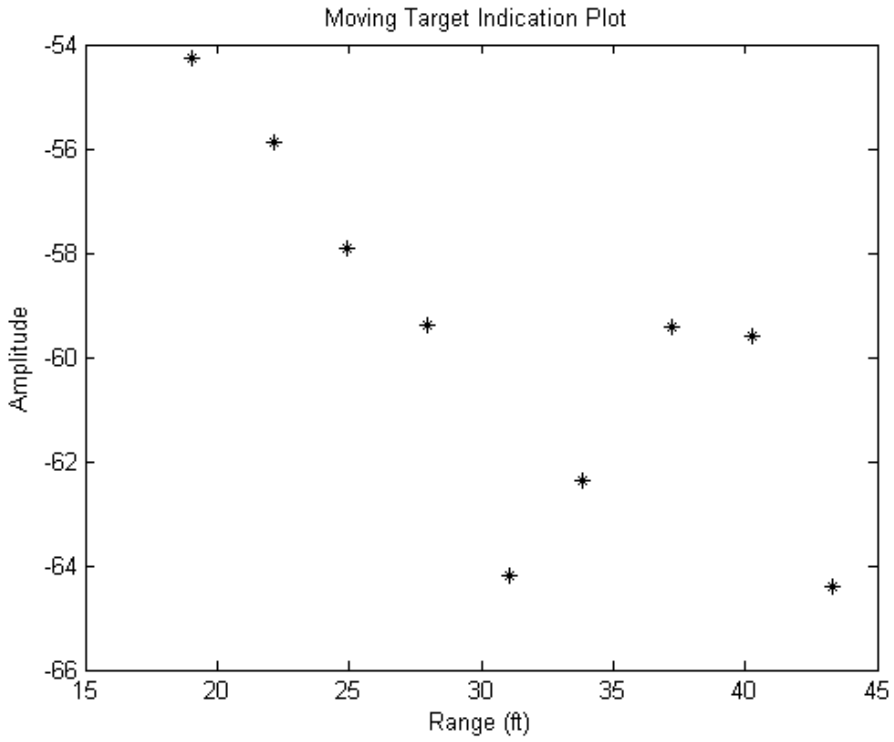

Figure 4–10: The maximum amplitude plot for all nine pulses showing the presence of the corner reflector.

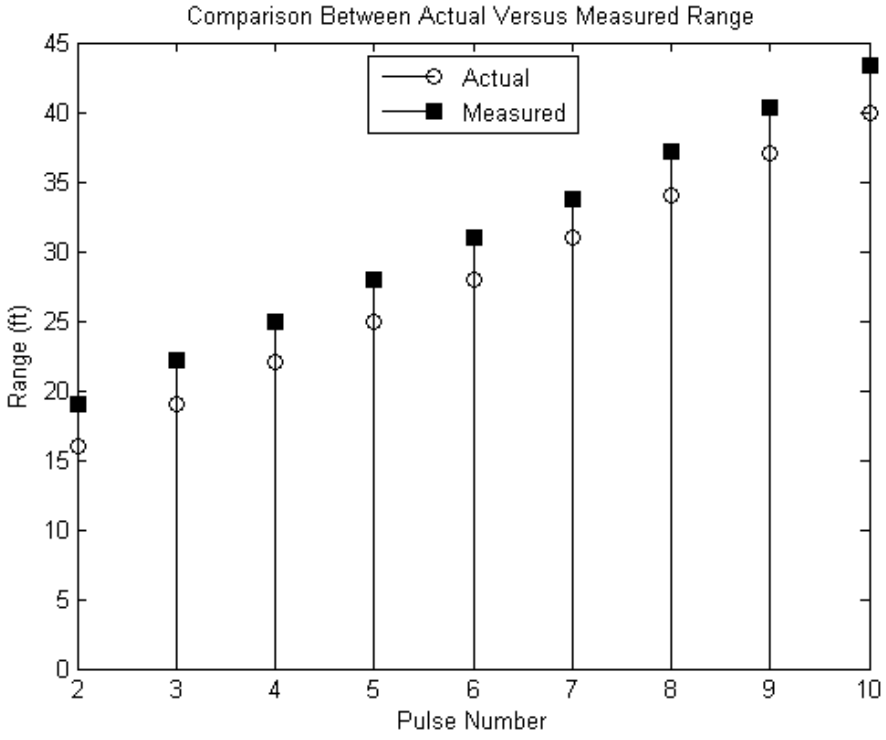

Figure 4–11: A comparison between the actual versus measured range information of the corner reflector in the hallway.

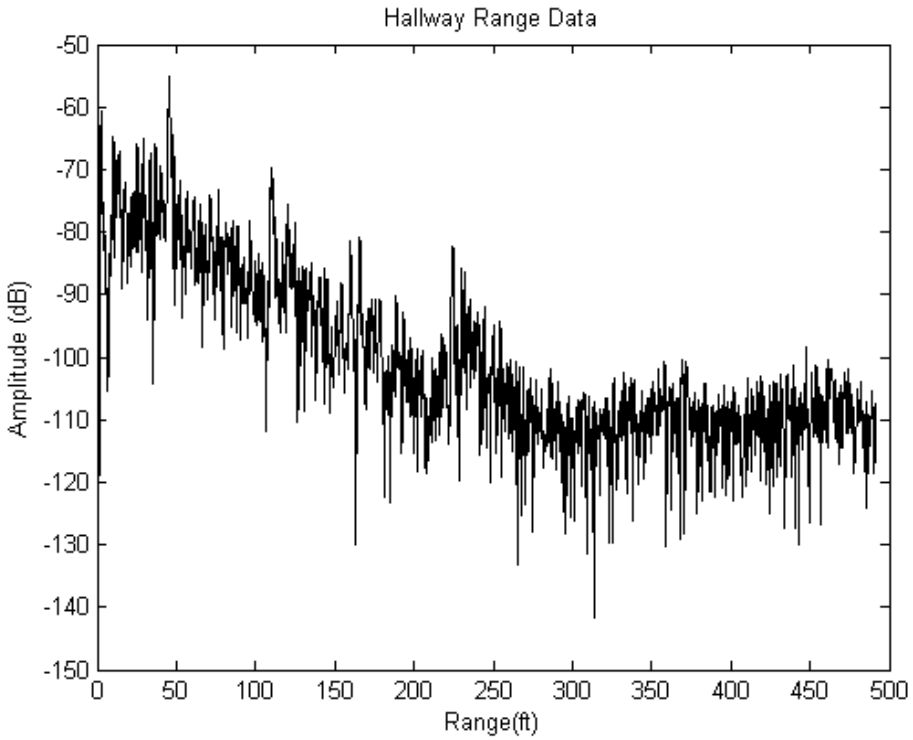

Figure 4–12: The hallway returns for the reference pulse for the sphere data with no target present.

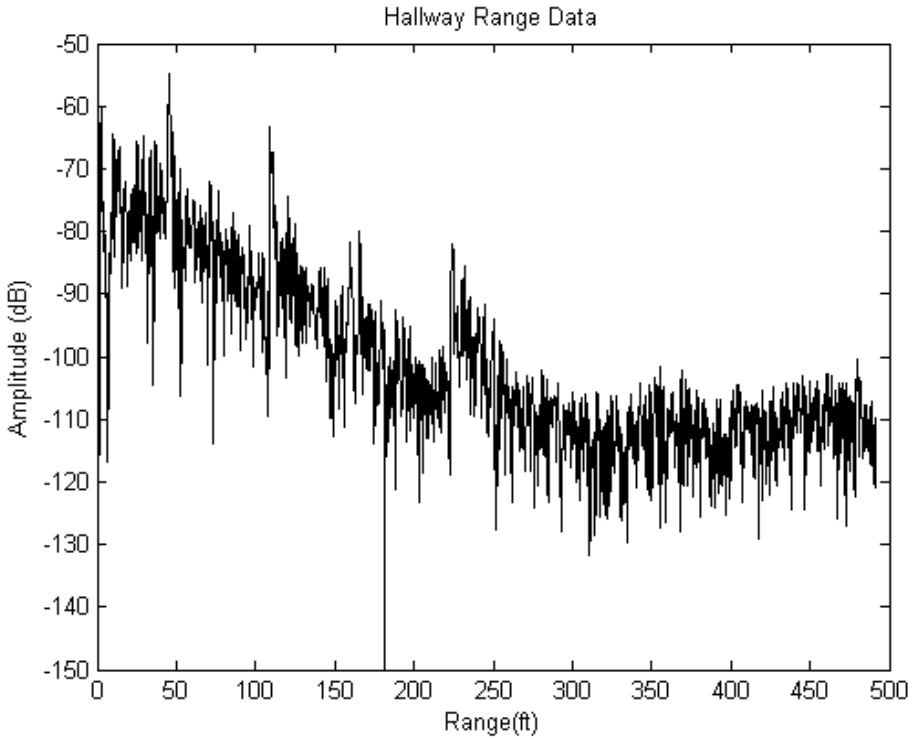

Figure 4–13: The hallway returns for the second pulse with the presence of the sphere.

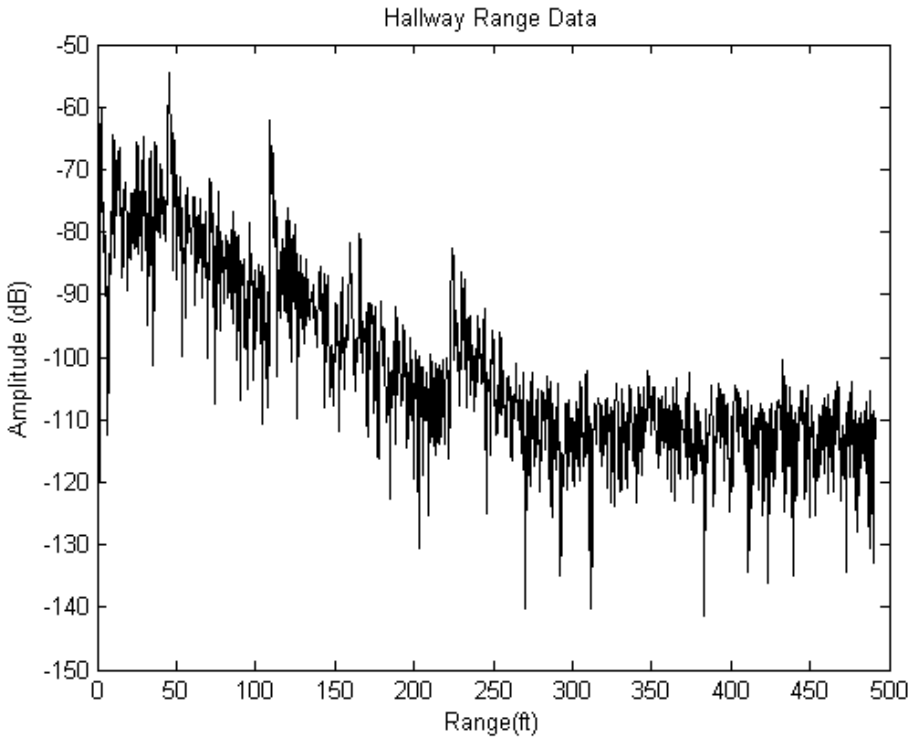

Figure 4–14: The hallway returns of the third pulse with the presence of the sphere.

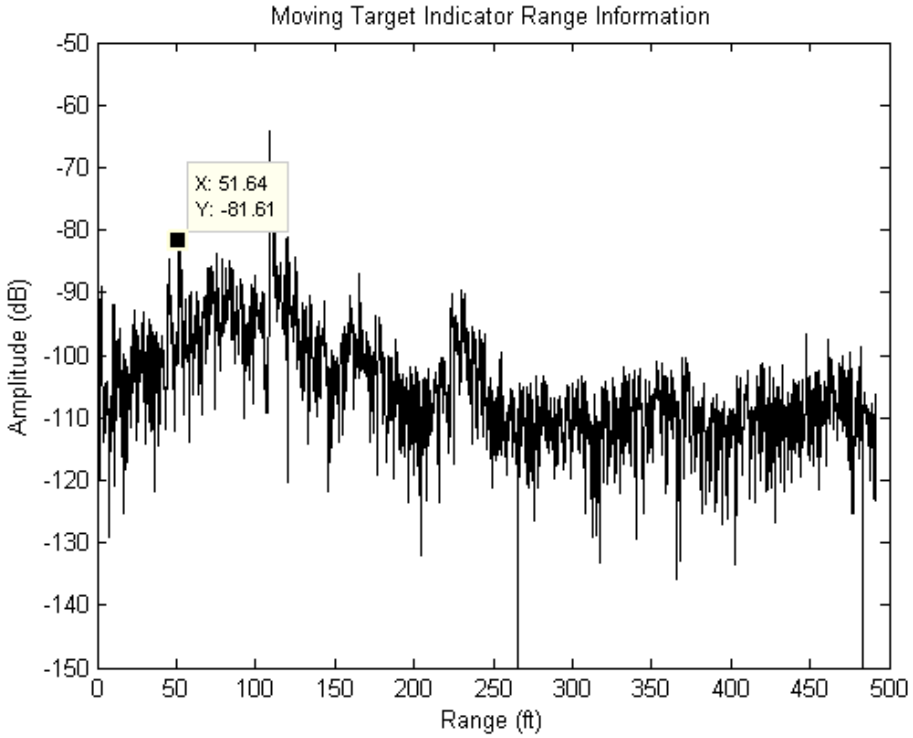

Figure 4–15: The pulse after cancelling between the second pulse and the reference pulse showing the presence of the sphere.

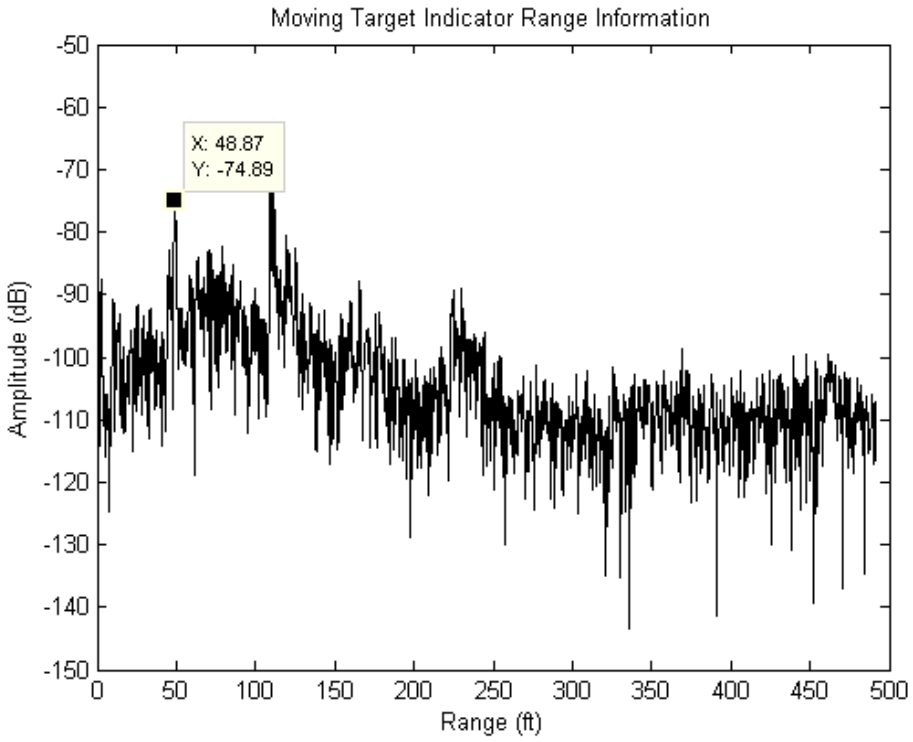

Figure 4–16: The pulse after cancelling between the third pulse and the reference pulse showing the presence of the sphere.

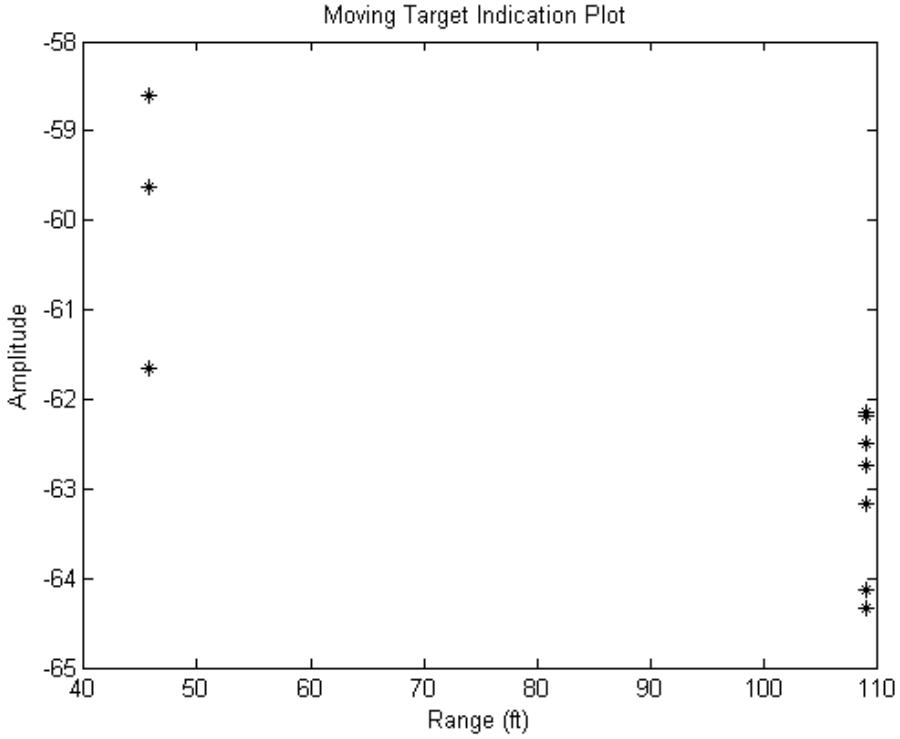

Figure 4–17: The maximum amplitude plot for ten pulses with the presence of each sphere in each pulse.

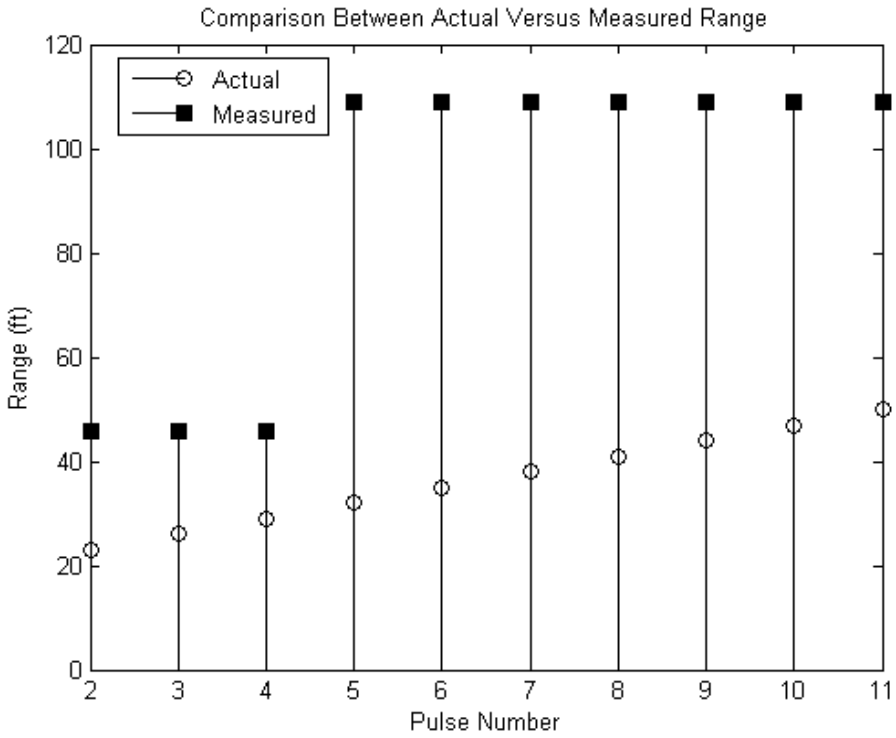

Figure 4–18: A comparison between the actual versus measured range information of the sphere in the hallway.

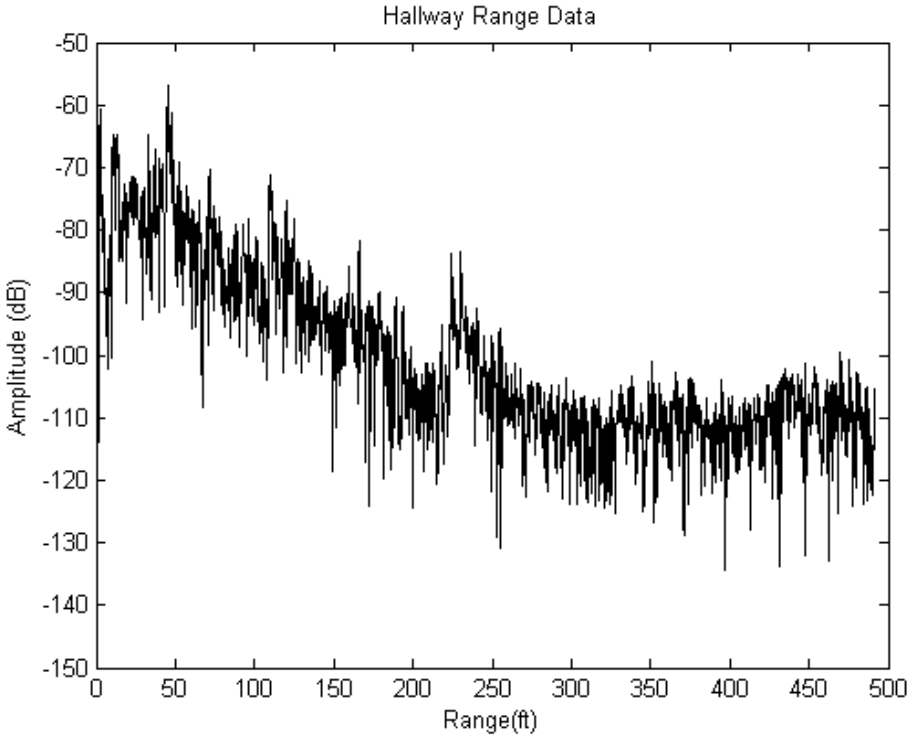

Figure 4–19: The hallway returns of the reference pulse without the presence of the human subject.

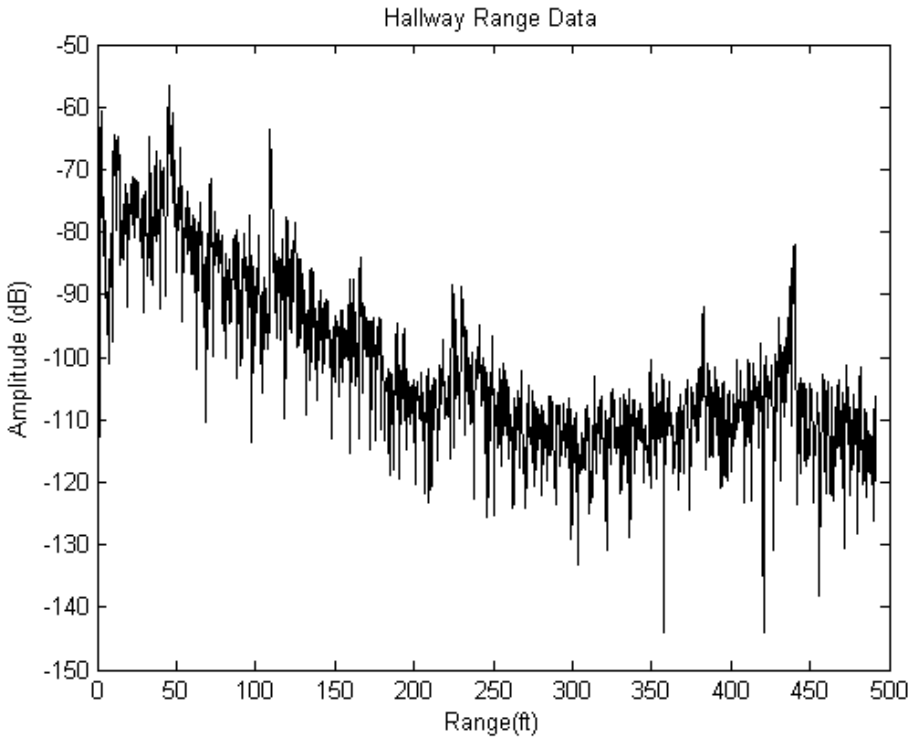

Figure 4–20: The hallway returns of pulse two with the presence of the human subject.

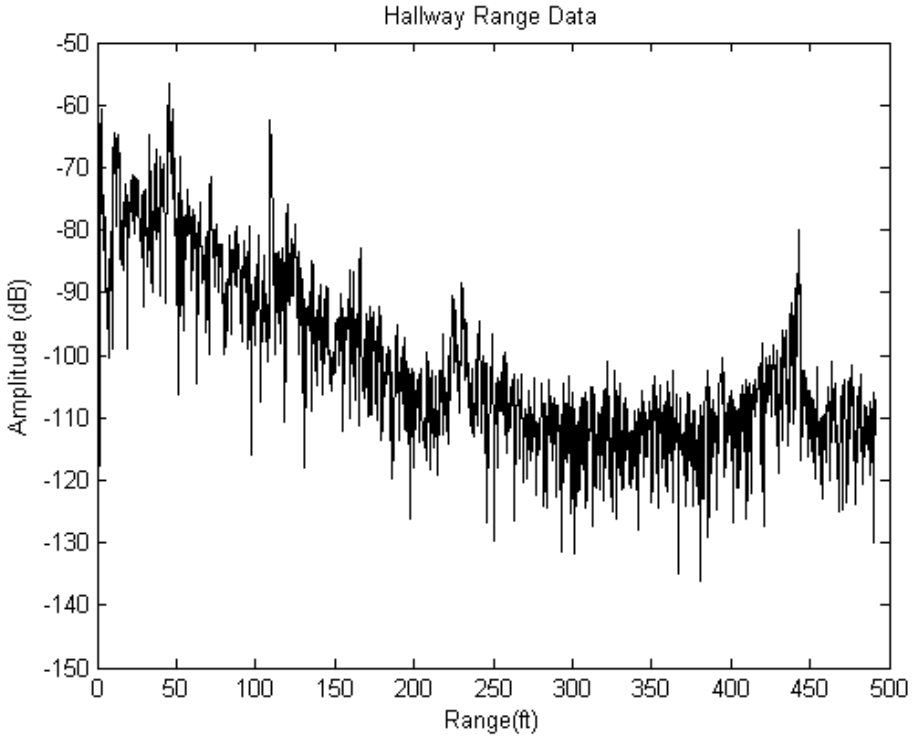

Figure 4–21: The hallway returns of pulse three with the presence of the human subject.

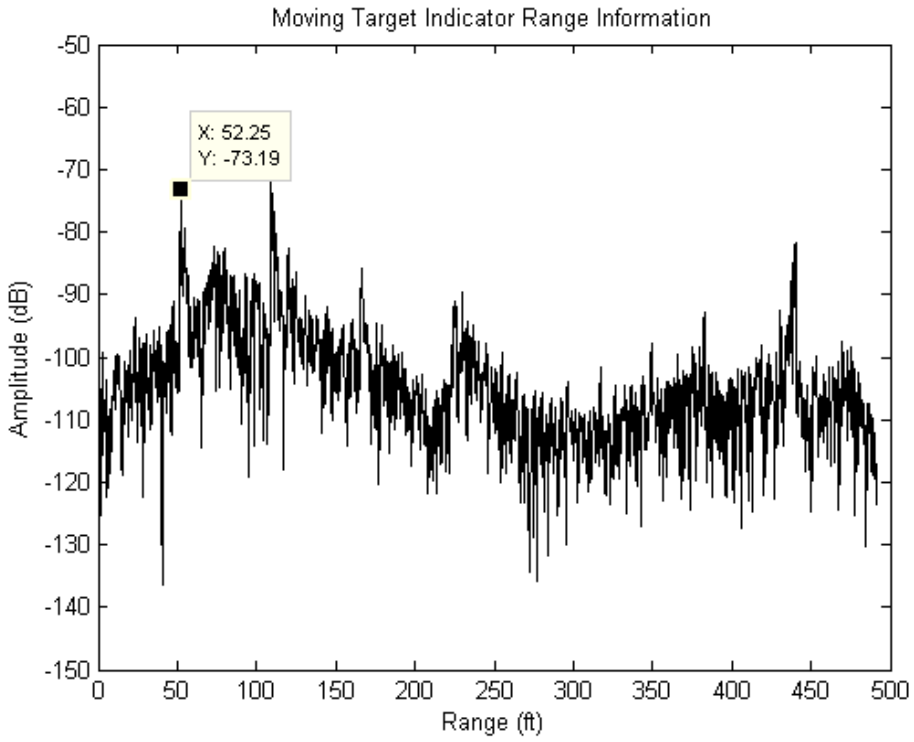

Figure 4–22: MTI cancellation between pulse two with the reference pulse showing the presence of the human.

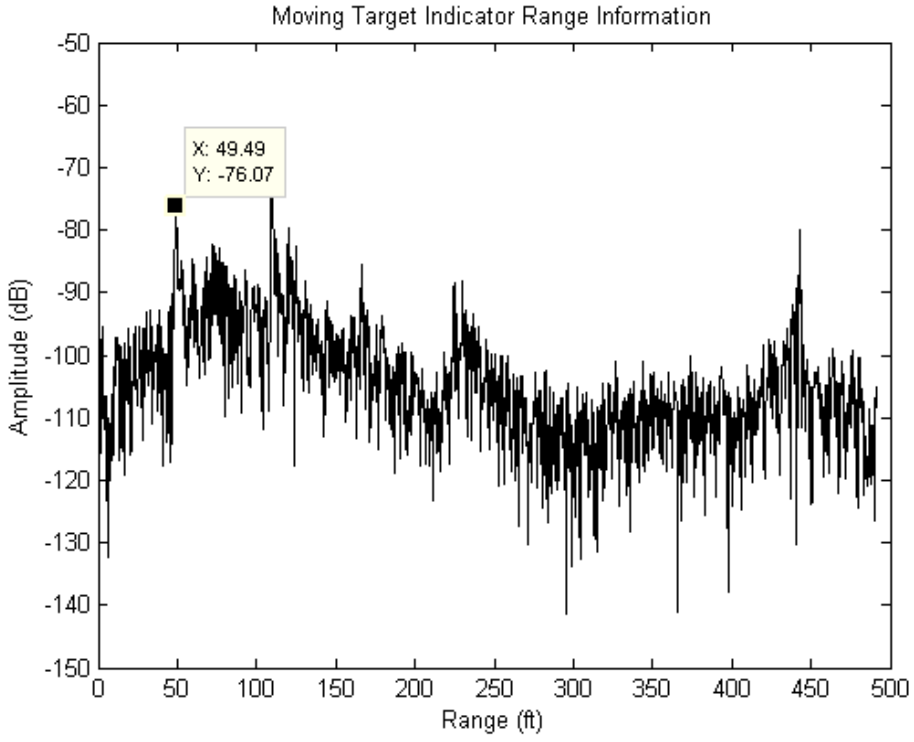

Figure 4–23: MTI cancellation between pulse three with the reference pulse showing the location of the human.

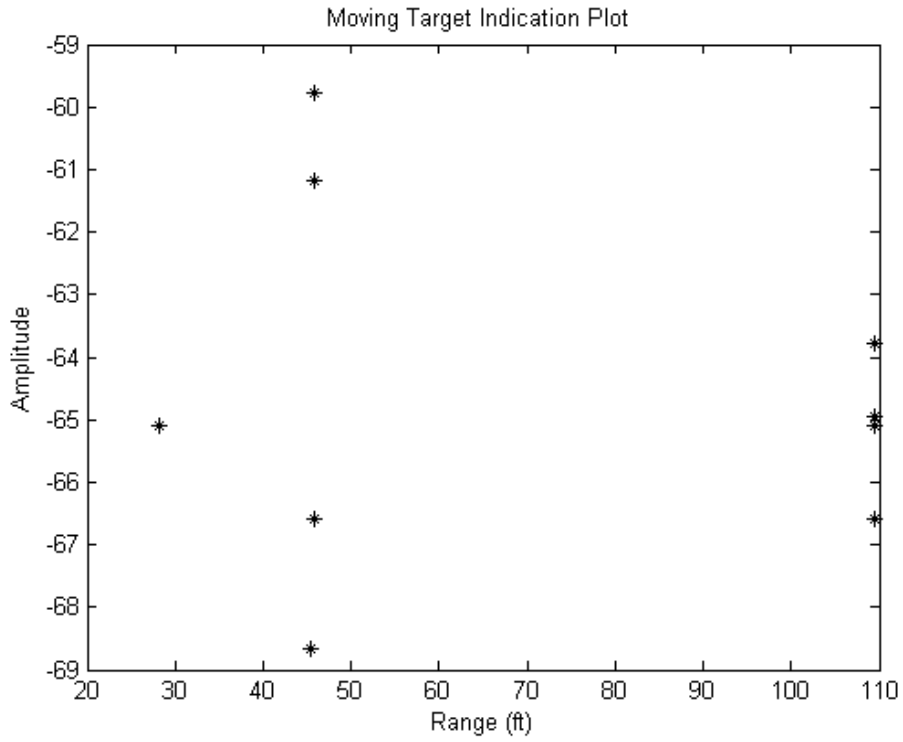

Figure 4–24: The maximum amplitude plot for ten pulses with the presence of the human subject in each pulse.

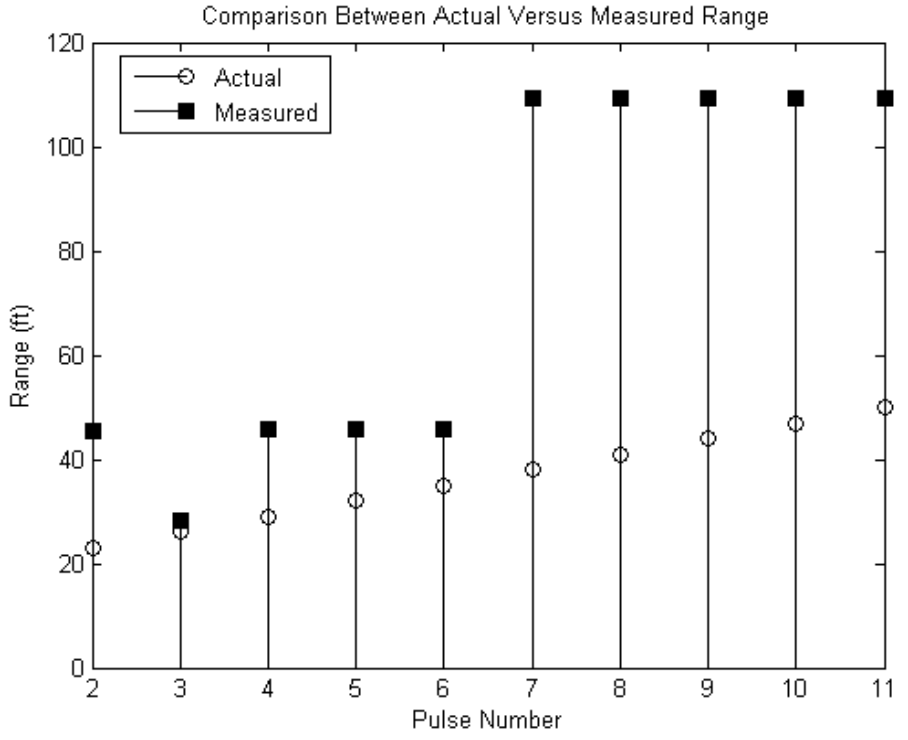

Figure 4–25: A comparison between the actual versus measured range information of the human subject in the hallway.

CHAPTER 5

CONCLUSIONS

There were several concepts demonstrated and proven to work for this project. Fundamental radar concepts of matched filtering and pulse compression were reviewed in Chapter 2, and a hardware implementation was validated in Chapter 3. The measurements in Chapter 3 confirmed that using a reference pulse in a variable delay MTI filter can successfully detect a target in a low clutter environment. The results of Chapter 4 revealed that a corner reflector, a sphere, or a human subject can be detected in a hallway where high clutter is prevalent using the proposed detection scheme.

The coherency of the entire system is the limiting factor in the proposed target detection method. If coherence was not maintained over an extended period of time, a variable delay MTI filter then could not be used. If a non-coherent radar system was used, after MTI cancellation it would be difficult to locate the target signal return. It is even possible that the phase of the target return could be completely cancelled making it impossible to see the target. However, the coherency measurements showed that the reference pulse could be updated every 15 minutes to two hours in the test environment. Someone trying to defeat the system by moving slowly would have to move less than a single range cell (approximately 3.7 inches) every 15 minutes to two hours to be successful. Moreover, this assumes the perpetrator would have prior knowledge of the refresh period of the reference pulse and the operating bandwidth of the radar system. Without that prior knowledge, this radar system should be successful in detecting a threat.

There were issues, however, that showed up in the measurement process. The system coherency test did prove the radar system stays coherent over a long period of time. Once a target was introduced into the test environment, whether it was the anechoic chamber or hallway, the main strong reflection points of the environment would still show up after cancellation. This was contrary to what was expected from the system coherency data. One possible explanation to this problem is that when the target is introduced into the environment, it adds additional delay to all of the range cells that fall behind the target due to multipath

propagation. But, this would mean at least an additional delay of 3.7 inches had to be added in. Another explanation could be the reflection magnitudes of the background reflectors change after the target is introduced into the environment. The target intercepts and scatters energy that would otherwise reflect from the background, preventing the hallway backscatter from being completely cancelled out. Either way, the changes in the cancellation data indicates that a target was present even if it could not be resolved in range. In any future work, this problem would need to be addressed.

Other future work would include automating the entire radar system. Also, to make the measurements more time efficient, a graphical user interface (GUI) would enable the radar operator to collect and analyze data more quickly. It would allow the operator to immediately see the results of the collected data. If there was a problem during the collection of the data, the operator could immediately repeat the results. Without the GUI, the operator would first have to transfer the data to a computer and run it through a program to see the results.

This test was a proof-of-concept. Therefore, it was only necessary to use the available equipment. In most radar systems, however, it is cheaper to build the radar from several hardware components. Using a VNA as a radar system can be expensive. Also, the VNA was designed and built to be a multi-faceted piece of equipment. It was not specifically designed to operate as a radar system. The performance of the radar system could be made better by specifically designing it to operate in a high clutter environment.

APPPENDIX A

MATLAB CODE

FMCW SWEEP

```
%David Gentry
% FMCW Sweep

clear

%Defining the frequency sweep in Hertz
Frequency=linspace(1, 3, 1000);

%Defining the time range (s)
time=linspace(0,3,1000);

%Defining the sinusoidal sweep function
x=sin(2.*pi.*Frequency.*time);

n=length(x);

%Mirroring the x function
for m=1:n

    y(m)=x(length(x)-m+1);

end

z=conv(x,y);

figure; plot(x,'k')
title('Linear Frequency Modulation Sweep')
ylabel('Amplitude')
xlabel('Samples')


figure; plot(abs(z),'k')
title('Output From A Matched Filter')
ylabel('Amplitude')
xlabel('Convolution Vector Length(2n-1)')
```

FOURIER TRANSFORM OF FMCW SWEEP

```
%David Gentry
% Fourier Transform of FMCW Sweep

clear

%Defining the frequency sweep in Hertz
Frequency=linspace(1, 3, 1000);

%Defining the time range (s)
time=linspace(0,3,1000);

%Defining the sinusoidal sweep function
x=sin(2.*pi.*Frequency.*time);

%Taking the Fourier Transform of x
x_freq_domain=fft(x);

%Taking the complex conjugate
H_Matched_Filter=conj(x_freq_domain);

%Finding the output signal
Y_Output=x_freq_domain.*H_Matched_Filter;

%Taking the inverse Fourier Transform
y=fftshift(ifft(Y_Output));

semilogy(abs(fftshift(x_freq_domain)),'k')
title('Fourier Transform of an FMCW Sweep')
xlabel('Frequency Points')
ylabel('Magnitude')
```

PULSE COMPRESSION

```
%Ernest David Gentry
%Pulse Compression Code
%ECEN 5000 Thesis - Radar Project

clear
clf;

c=2.99792458e8;  %Speed of light in a vacuum (m/s).

Range_Max=20; %Maximum range of target in meters(m).
R_Target1 = 19; %Range of target 1.

Time_Delay_Max=2.*Range_Max./c; %Maximum time delay in seconds (s).
```

```
Frequency_Step=1./Time_Delay_Max; %Defining the step frequency value
(Hz).

Frequency_Sweep=3.3e9:Frequency_Step:4.9e9; %Sweeping over specified
frequency range (Hz).

N_Samples=length(Frequency_Sweep); %Find the number of frequency steps.

IndexOne=find(Frequency_Sweep,1, 'first');
IndexTwo=find(Frequency_Sweep,1, 'last');

Frequency_Bandwidth=abs(Frequency_Sweep(IndexTwo)-...
    Frequency_Sweep(IndexOne)); %Finding the sweep bandwidth (Hz).

Time_Step=1./(2.*Frequency_Bandwidth); %Defining the step time value
(s).

Time_Sweep=0:Time_Step:(N_Samples-1).*Time_Step; %Defining the time
axis for the inverse Fourier Transform.

Beta_z=-2.*pi.*Frequency_Sweep.*Range_Max./c; %Finding the phase value
for each frequency value.
Beta_z1 = -2.*pi.*Frequency_Sweep.*R_Target1./c;

%Calculating the received phasor.
Received_Phasor=50.*exp(j.*2.*Beta_z1);

Time_Domain=ifft(Received_Phasor);

Time_Domain_Max=abs(max(Time_Domain));

Index_Time_Domain=find(abs(Time_Domain)-Time_Domain_Max==0,...
    1,'last'); %Finding the index value that has the maximum amplitude.

Time_Delay=Time_Sweep(Index_Time_Domain);

subplot 211
stem(Frequency_Sweep, real(Received_Phasor),'k')
title('Plot of the Complex Phasor')
xlabel('Frequency(Hz)')
ylabel('I Channel')
xlim([3.3e9 4.9e9])
subplot 212
stem(Frequency_Sweep, imag(Received_Phasor),'k')
xlabel('Frequency (Hz)')
ylabel('Q Channel')
xlim([3.3e9 4.9e9])

figure; stem(Time_Sweep.*c, abs(Time_Domain),'k');
title('Time Domain')
ylabel('Amplitude')
xlabel('Range (m)')
xlim([0 Range_Max])
```

SYSTEM COHERENCY CODE

```
%David Gentry
%ECEN 5000 - Thesis
%Moving Target Indicator Program

clear

Pulses = 11; %Number of pulses

%Creating a Hanning Window
W = window(@hann,1601);
W1=W.';
TD_Diff=zeros(1,1601);

for A=1:Pulses

    if A>5

        Num_Str = '';

    else

        Num = 0;
        Num_Str = num2str(Num);

    end

    Num_Real=2*A-2;
    Num_Str_Real=num2str(Num_Real);
    Num_Imag = 2*A-1;
    Num_Str_Imag=num2str(Num_Imag);

    DIR = 'C:\Users\Alan\Documents\ECEN 5000 Thesis Project';
    DIR2 = '\Hallway\Moving Target Measurements\System Coherency\TXT1';
    DIR_EXT = '.csv';

    Load_File_Real = strcat(DIR, DIR2,Num_Str,Num_Str_Real,DIR_EXT);
    Load_File_Imag = strcat(DIR, DIR2,Num_Str,Num_Str_Imag,DIR_EXT);

    % Importing the real part of the s21 parameter.
    S21_Real_Data =csvread(Load_File_Real,12,0);
    S21_Real = S21_Real_Data(1:length(S21_Real_Data), 2,:).';

    % Importing the imaginary part of the S21 parameter.
    S21_Imaginary_Data =csvread(Load_File_Imag,12,0);
    S21_Imaginary =
      S21_Imaginary_Data(1:length(S21_Imaginary_Data),2,:).';

    % Turning the S21 parameter back into a complex number.
    S21_Complex(A,:)=W1.*(S21_Real + 1i.*S21_Imaginary);

    %Subtracting the original pulse from the current pulse
    TD_Diff = ifft(S21_Complex(A,:)) - TD_Diff;
```

```
    TD_Diff2 = ifft(S21_Complex(A,:)) - ifft(S21_Complex(1,:));

    %Dumping the d
    TD(A,:) = TD_Diff;
    TD2(A,:) = TD_Diff2;
    TD_Diff = TD(1,:);

    %Recovering the time domain data
    Time_Domain(A,:) = ifft(S21_Complex(A,:));

end

%% System Settings

c = 186282.*5280;    %Speed of light in a vacuum (ft/s).

%Importing the frequency data
S21_Freq_Range = S21_Real_Data(1:length(S21_Real_Data), 1,:).';

% Finding the frequency step
Freq_Diff = S21_Freq_Range(2)-S21_Freq_Range(1);

% Finding the number of frequency steps.
N_Samples=length(S21_Freq_Range);

% Finding the sweep bandwidth (Hz).
IndexOne=find(S21_Freq_Range,1, 'first');
IndexTwo=find(S21_Freq_Range,1, 'last');
Frequency_Bandwidth=abs(S21_Freq_Range(IndexTwo)-...
    S21_Freq_Range(IndexOne));

% Finding the time step for each N point
Time_Step = 1./Frequency_Bandwidth;
delta_Range = c.*Time_Step./2;

% Calculating the time base for the recovered time domain signal.
Time_Sweep=0:Time_Step:(N_Samples-1).*Time_Step;

% Converting the time base into a target range values (m)
Range_Values = c.*Time_Sweep./2;

for B = 1:Pulses

    mean_Amp = mean(abs(TD2(B,:)));

    figure; plot(Range_Values, 20.*log10(abs(TD2(B,:))),'k')
    title(sprintf(['System Coherency Measurement Between Pulses 1 &
%g',...
        '\n','Mean Amplitude = %g'],B,mean_Amp))
    xlabel('Range (ft)')
    ylabel('Amplitude')
    ylim([-150 -50])

end
```

MOVING TARGET INDICATION CODE

```
%David Gentry
%ECEN 5000 - Thesis
%Moving Target Indicator Program

clear

Pulses = 10; %Number of pulses

%Creating a Hanning Window
W = window(@hann,1601);
W1=W.';
TD_Diff=zeros(1,1601);

for A=1:Pulses

    if A>5

        Num_Str = '';

    else

        Num = 0;
        Num_Str = num2str(Num);

    end

    Num_Real=2*A-2;
    Num_Str_Real=num2str(Num_Real);
    Num_Imag = 2*A-1;
    Num_Str_Imag=num2str(Num_Imag);

%       DIR = 'C:\Users\Alan\Documents\ECEN 5000 Thesis Project';
%       DIR2 = '\Anechoic Chamber\Corner Reflector\TXT1';
%       DIR_EXT = '.csv';
%
%       DIR = 'C:\Users\Alan\Documents\ECEN 5000 Thesis Project';
%       DIR2 = '\Anechoic Chamber\Sphere\TXT1';
%       DIR_EXT = '.csv';

    DIR = 'C:\Users\Alan\Documents\ECEN 5000 Thesis Project';
    DIR2 = '\Hallway\Moving Target Measurements\Toward Radar Part
      2\TXT1';
    DIR_EXT = '.csv';
    Measured_Target_Range_Ft = [16 19 22 25 28 31 34 37 40];

% %
%     DIR = 'C:\Users\Alan\Documents\ECEN 5000 Thesis Project';
%     DIR2 = '\Hallway\Moving Target Measurements\Toward Radar Human
      Target\TXT1';
%     DIR_EXT = '.csv';
%     Measured_Target_Range_Ft = [23 26 29 32 35 38 41 44 47 50];
%
%     DIR = 'C:\Users\Alan\Documents\ECEN 5000 Thesis Project';
```

```
%     DIR2 = '\Hallway\Moving Target Measurements\Toward Radar Sphere
Target\TXT1';
%     DIR_EXT = '.csv';
%     Measured_Target_Range_Ft = [23 26 29 32 35 38 41 44 47 50];
%
%     DIR = 'C:\Users\Alan\Documents\ECEN 5000 Thesis Project';
%     DIR2 = '\Hallway\Moving Target Measurements\Antenna Delay\TXT1';
%     DIR_EXT = '.csv';

    Load_File_Real = strcat(DIR, DIR2,Num_Str,Num_Str_Real,DIR_EXT);
    Load_File_Imag = strcat(DIR, DIR2,Num_Str,Num_Str_Imag,DIR_EXT);

    % Importing the real part of the s21 parameter.
    S21_Real_Data =csvread(Load_File_Real,12,0);
    S21_Real = S21_Real_Data(1:length(S21_Real_Data), 2,:).';

    % Importing the imaginary part of the S21 parameter.
    S21_Imaginary_Data =csvread(Load_File_Imag,12,0);
    S21_Imaginary =
      S21_Imaginary_Data(1:length(S21_Imaginary_Data),2,:).';

    % Turning the S21 parameter back into a complex number.
    S21_Complex(A,:)=W1.*(S21_Real + 1i.*S21_Imaginary);

    %Subtracting the original pulse from the current pulse
    TD_Diff = ifft(S21_Complex(A,:)) - TD_Diff;
    TD_Diff2 = ifft(S21_Complex(A,:)) - ifft(S21_Complex(1,:));

    %Dumping the d
    TD(A,:) = TD_Diff;
    TD2(A,:) = TD_Diff2;
    TD_Diff = TD(1,:);

    %Recovering the time domain data
    Time_Domain(A,:) = ifft(S21_Complex(A,:));

end

%% System Settings

c = 186282.*5280; %Speed of light in a vacuum (ft/s)

%Importing the frequency data
S21_Freq_Range = S21_Real_Data(1:length(S21_Real_Data), 1,:).';

% Finding the frequency step
Freq_Diff = S21_Freq_Range(2)-S21_Freq_Range(1);

% Finding the number of frequency steps.
N_Samples=length(S21_Freq_Range);

% Finding the sweep bandwidth (Hz).
IndexOne=find(S21_Freq_Range,1, 'first');
IndexTwo=find(S21_Freq_Range,1, 'last');
```

```
Frequency_Bandwidth=abs(S21_Freq_Range(IndexTwo)-...
    S21_Freq_Range(IndexOne));

% Finding the time step for each N point
Time_Step = 1./Frequency_Bandwidth;
delta_Range = c.*Time_Step./2;

% Calculating the time base for the recovered time domain signal.
Time_Sweep=0:Time_Step:(N_Samples-1).*Time_Step;

% Converting the time base into a target range values (m)
Range_Values = c.*Time_Sweep./2;

for B = 1:Pulses

    mean_Amp = mean(abs(TD2(B,:)));

    figure; plot(Range_Values, 20.*log10(abs(TD2(B,:))),'k')
    title('Moving Target Indicator Range Information')
    xlabel('Range (ft)')
    ylabel('Amplitude')
    ylim([-150 -50])

    figure; plot(Range_Values, 20.*log10(abs(Time_Domain(B,:))),'k')
    title('Hallway Range Data')
    xlabel('Range(ft)')
    ylabel('Amplitude')
    ylim([-150 -50])

end

%% Moving Target Indication

Index_Range = zeros(1,Pulses-1);
Target_Range = zeros(1,Pulses-1);
Target_Amplitude = zeros(1,Pulses-1);

for C = 2: Pulses

    [Amp I] = max(abs(TD(C,1:800)));

    Index(C-1) = I;
    Amplitude(C-1) = Amp;

end

Pulse_Num = linspace(2,Pulses,Pulses-1);
Target_Range = Range_Values(Index);


figure;
stem(Target_Range, Amplitude,'k')
title('Moving Target Indication Plot ')
```

```
xlabel('Range (ft)')
ylabel('Amplitude')

figure;
stem(Pulse_Num, Measured_Target_Range_Ft,'k')
hold on
stem(fliplr(Pulse_Num), Target_Range,'fill','k','Marker','square')
legend('Actual','Measured','Location','Best')
title('Comparison Between Actual Versus Measured Range')
xlabel('Pulse Number')
ylabel('Range (ft)')
hold off
```

VITA

Ernest David Gentry

Candidate for the Degree of

Master of Science

Thesis: LOCATING A MOVING TARGET IN A HIGH CLUTTER ENVIRONMENT

Major Field: Electrical Engineering

Biographical:

Personal Data:

David Gentry was 26 years old when he finished in Master's degree in electrical engineering. His hobbies include coin collecting, hiking, reading books, and playing video games.

Education:

Completed the requirements for the Master of Science in Electrical Engineering at Oklahoma State University, Stillwater, Oklahoma in December, 2010.

Completed the requirements for the Bachelor of Science in Electrical Engineering at Oklahoma State University, Stillwater, Oklahoma in December, 2007.

Experience:

He helped in building and testing a radar system for the Microwave Engineering course taught at Oklahoma State University.

He interned at Boeing with the Electromagnetic Effects department writing a test plan and procedure for the E-4B Airforce aircraft.

Professional Memberships:

Eta Kappa Nu

Name: Ernest David Gentry Date of Degree: December, 2010

Institution: Oklahoma State University Location: Stillwater, Oklahoma

Title of Study: LOCATING A MOVING TARGET IN A HIGH CLUTTER ENVIRONMENT

Pages in Study: 67 Candidate for the Degree of Master of Science

Major Field: Electrical Engineering

Scope and Method of Study:

This paper addresses the problem of locating a slowly moving target, such as a human being, in a high clutter environment. The test uses a vector network analyzer (VNA) as a radar system. The radar system is operated as a frequency-stepped continuous wave (FSCW) radar. The real and imaginary amplitude values of the S21 parameter are recorded for each frequency step. The inverse fast-Fourier transform (IFFT) is then applied to the complex S21 data to recover the time domain returns from a room or hallway. The target is located using a variable pulse repetition frequency (PRF) moving target indicator (MTI) filter. A reference pulse of the room or hallway was acquired, initially, with no target present. Consecutive pulses were then measured with the target present in the room or hallway. After each pulse, the target was moved 3 ft and a new measurement was saved. This process was repeated for each target. Targets included a corner reflector, a sphere, and a human subject.

Findings and Conclusions:

The results showed that the variable PRF, single-stage, MTI filter effectively identified the presence of a target in a high clutter environment for all three target cases. Subtracting a reference pulse from the pulses when a target was present in the room or hallway suppressed most of the background clutter. There were some returns from strong reflection points in the room or hallway that still appeared in the filter returns, however. This was due to either the target intercepting and scattering the energy that would otherwise reflect from the background or the range cells of the background return signals being moved due to multipath.

This test demonstrated that use of a reference pulse in a variable PRF MTI filter allowed the detection of a slowly moving target. Future work will be needed to address the issue of strong reflection points appearing after filtering. Possible solutions include addition of a second MTI stage to the processing.

ADVISER'S APPROVAL: Dr. James West